NASA Technical Memorandum 88917

A Comparative Study of Some Dynamic Stall Models

T.S.R. Reddy
The University of Toledo
Toledo, Ohio

and

K.R.V. Kaza
Lewis Research Center
Cleveland, Ohio

March 1987

NASA

A COMPARATIVE STUDY OF SOME DYNAMIC STALL MODELS

T.S.R. Reddy*
The University of Toledo
Toledo, Ohio 43606

and

K.R.V. Kaza
National Aeronautics and Space Administration
Lewis Research Center
Cleveland, Ohio 44135

E-3342

SUMMARY

Three semi-empirical aerodynamic stall models are compared with respect to their lift and moment hysteresis loop predication, limit cycle behavior prediction, easy implementation, and feasibility in developing the parameters required for stall flutter prediction of advanced turboprops. For the comparison of aeroelastic response prediction including stall, a typical section model and a plate structural model are considered. The response analysis includes both plunging and pitching motions of the blades.

In model A, a correction to the angle of attack is applied when the angle of attack exceeds the static stall angle. In model B, a synthesis procedure is used for angles of attack above static stall angles and the time history effects are accounted through the Wagner function. In both models the lift and moment coefficients for angles of attack below stall are obtained from tabular data for a given Mach number and angle of attack. In model C, referred to as the ONERA model, the lift and moment coefficients are given in the form of two differential equations, one for angles below stall and the other for angles above stall. The parameters of these equations are nonlinear functions of the angle of attack. The effects of vortex-shedding, an important feature of dynamic stall, are not considered in model A, accurately considered in model B, and approximately considered in model C. However, it is observed that the high frequency, low amplitude oscillations, sweep, and high subsonic Mach number operating environment of advanced turboprops favor light stall conditions where the effect of vortex-shedding is less severe. This permits the use of simple models like models A and C in the stall flutter analysis of advanced turboprops.

INTRODUCTION

Highly-loaded propellers, called advanced turboprops, are proposed to power transport aircraft at high subsonic speeds. The renewed interest in the propeller is brought about by the significant benefits in fuel consumption. Flutter analysis of these turboprops is needed to determine the critical (flutter) speed below which the aircraft has to operate to avoid catastrophic failure. A response analysis is needed to determine the loads on the blades and fatigue life of a turboprop. Figure 1 shows a typical advanced turboprop

---

*NASA Resident Research Associate.

wind tunnel model. The blade is made thin to increase the drag divergence Mach number, and is swept to reduce the local effective Mach number. The sweep introduces a large degree of coupling between bending and torsion, which alters the aeroelastic behavior. In addition, to hold propeller diameter to a reasonable value, and to have high disk loading, a large number of blades are provided for the advanced turboprop. Consequently the turboprop has to be analyzed accounting for aerodynamic interaction between the blades. The aeroelastic response and flutter analysis of advanced turboprops is an ongoing research effort at NASA Lewis Research Center.

Under normal conditions (ref. 1), the blade sections of a conventional propeller are at low angles of attack, the flutter speed is high, and generally there is an appreciable margin of safety between the operating speed and the flutter speed. However, during the take-off period, the propeller blade sections may operate at high angles of attack and could be subjected to stall flutter, a self-sustained vibration in a periodically separated flow condition. The flutter speed at this condition is very low, and stall flutter affects the fatigue life of the turboprop. Hence, predicting this stall flutter speed is a critical design task, and an appropriate method of analysis of stall flutter is a critical research need. Prediction of flutter speeds at low angles of attack (classical flutter) for advanced turboprops has been performed by modifying the existing analysis methods as described in reference 2. Both analytical and experimental results are presented in reference 3. Recently, additional experimental flutter data was presented in reference 4. The analyses included the effect of number of blades (cascades) and the blade sweep. However, the studies on stall flutter are few and mostly empirical. This is due to the complexity in modeling the flow in a periodically separated flow state.

The objective of the present effort is to develop stall flutter models for advanced turboprops. As a part of this general effort, the available dynamic stall models are reviewed and applied to simple structural models to study the extent of their validity, and to select an appropriate model for advanced turboprop application. In this report, three dynamic stall models are used together with typical section and plate structural models. Their performance is investigated from the view point of lift and moment hysteresis loop prediction, limit cycle prediction, easy implementation and the feasibility of developing the corresponding stall models for arbitrary airfoils. The plate model in conjunction with its normal modes is considered in order to explore whether the analytical integration of the loads in the blade spanwise direction is feasible. The numerical study is performed for a single blade and cascade effects are not included.

NOMENCLATURE

A	nondimensional rate of angle of attack, $c\dot{\alpha}/2V$
a	empirical parameter, equations (20b), and (20e)
a_h	distance between midchord and elastic axis, measured in semichords positive towards the trailing edge.
$a_{0\ell}$	static lift curve slope

a_{om}	static pitching moment curve slope at zero angle of attack
b	semi-chord, m
C_{L1}	lift coefficient in linear range, equation (20a)
C_{L2}	lift coefficient in nonlinear range, equation (20b)
$C_{L\ell}$	lift coefficient given by linear relation, equation (20a)
C_{LS}	static lift coefficient
C_{LU}	unsteady c_ℓ, equation (18a)
C_{M1}	moment coefficient in linear range, equation (20d)
C_{M2}	moment coefficient in nonlinear range, equation (20e)
$C_{M\ell}$	moment coefficient given by linear relation, equation (20d)
C_{MS}	static moment coefficient
C_{MU}	unsteady c_m, equation (19a)
C_N	normal force coefficient
c	chord length, m
c_ℓ	aerodynamic lift force coefficient
$c_{mc/4}$	aerodynamic moment coefficient about quarter chord
c_m	aerodynamic moment coefficient about elastic axis
E	empirical parameter, equation (19a)
h	plunging degree of motion, positive downwards
I_α	polar moment of inertia of airfoil mass about elastic axis
K_α	torsional stiffness coefficient corresponding to pitching displacement
K_h	bending stiffness coefficient corresponding to plunging displacement
K_1	unsteady aerodynamic empirical factor, equation (3)
k	reduced frequency, based on semi-chord
ℓ	length of the plate, m
M	Mach number, normal to leading edge
m	mass of the airfoil per unit span

N	number of blade segments
NM	number of normal modes
P_1, P_2, P_3	empirical parameters for C_{LU}, equation (18b)
Q_α	total aerodynamic moment about elastic axis, positive nose up
Q_h	total aerodynamic lifting force, positive downwards
$Q_1, Q_2, \ldots Q_7$	empirical parameters for C_{LU}, equations (18d)
Re	Reynold's number
r_α	$\sqrt{I_\alpha/mb^2}$, radius of gyration about elastic axis in semi-chords
r	empirical parameter, equation (20b); radial distance on the blade
S	airfoil static moment about elastic axis
s_m	nondimensional time measured from instant of stall onset
s_{mt}	predicted value of s_m when vortex leaves trailing edge, equation (16)
s, τ	reduced time, Vt/b; also empirical parameter, equation (20a)
t	thickness of the airfoil; time
$\bar{t}$	ωt, nondimensional time parameter
t/c	airfoil thickness to chord ratio
t_{dm}	time when dynamic stall first occurs
U^*	nondimensional flight speed parameter
V	resultant velocity = $\sqrt{\Omega^2 r^2 + V_\infty^2}$, m/sec
V_∞	free stream velocity, m/sec
$\bar{x}_\alpha$	S/mb, distance between the elastic axis and the mass center measured in semi-chord, positive towards the trailing edge
α	instantaneous angle of attack; pitching degree of motion, positive nose up
$\bar{\alpha}$	amplitude of oscillation, deg
α_{Dm}	dynamic moment stall angle, equation (15), deg
α_E	effective angle of attack, deg, equation (1)
α_w	decay parameter, equation (3)

α_{RE}	angle of dynamic reattachment, equation (17), deg
α_{TE}	angle of attack when vortex near trailing edge
α_o	mean or initial angle of attack, deg
α_{ss}	static stall angle, deg
β	Prandtl-Glauert number
β_1	empirical constant, equation (18e) normally equals 0.18
γ	stall delay function, equation (2)
$\gamma_1;\gamma_2$	functions defined in equations (4) and (5)
$\Delta\alpha_1$	shift in angle, equation (18b), deg
$\Delta\alpha_2$	shift in angle, equation (18c), deg
$\Delta\alpha_{DS}$	incremental dynamic stall angle, equation (1)
ΔC_L	difference between static lift and extended linear lift
$\Delta C_{L1}, \Delta C_{L2}$	incremental lift coefficients, equations (18d) and (18e)
ΔC_M	difference between static moment and extended linear moment
ΔC_m	incremental moment coefficient, equation (19b)
δ_1, δ_2	dynamic parameters, equation (18g)
$\epsilon, C_{Am}, C_{wm}, C_{At}$ $C_{\alpha t}, C_{AR}, C_{wR}$	empirical parameters, equations (16) to (18)
$n_1, n_2 \ldots n_7$	empirical parameters for C_{MU}, equation (19b)
λ	empirical parameter, equation (20a)
μ	$m/\pi\rho b^2$ airfoil-air mass ratio
ξ	nondimensional plunging displacement
ρ	free stream air density
ζ_h	damping parameter in plunging motion
ζ_α	damping parameter in pitching motion
σ	empirical parameter, equation (20a)
$\phi_C(s,M)$	Wagner function, equation (14)
Ω	rotation speed, rad/sec

ω	frequency of harmonic oscillation, rad/sec
ω_α	$\sqrt{(K_\alpha/I_\alpha)}$ uncoupled pitching frequency of airfoil, rad/sec
ω_h	$\sqrt{(K_h/m)}$ uncoupled plunging frequency of airfoil, rad/sec
sign()	sign of ( ): either positive or negative
$()^\circ$	$\partial()/\partial t$
$()'$	$\partial()/\partial \bar{t}$
$()^*$	$\partial()/\partial \tau$ or $\partial()/\partial s$
$\lceil\rfloor$	diagonal matrix
[]	matrix

Stall, Dynamic Stall and Stall Flutter

As the angle of attack of an airfoil increases, the lift coefficient starts increasing. After a certain value of the angle of attack is reached, however, the lift drops suddenly because the flow over the airfoil separates. This is the condition of stall. This separation process depends on the airfoil shape (leading edge radius), thickness, Reynold's number, maximum thickness position, and Mach number. It has been recognized (refs. 5 and 6) that there are three principal types of stall: (1) trailing edge stall, where there is a gradual loss of lift at high lift coefficient as the boundary layer separation progresses gradually forward from the trailing edge, (2) leading edge stall, where there is an abrupt loss of lift, as the angle of attack for maximum lift is exceeded, with little or no rounding over of the lift curves; and is associated with the bursting of a laminar leading edge separation bubble, and (3) thin airfoil stall, where there is a gradual loss of lift even at low lift coefficients, and develops when a separation bubble originates near the leading edge and lengthens progressively as the angle of attack increases. The behavior of the lift coefficient in each type of static stall is shown in figure 2. It has also been found that trailing edge stall occurs for airfoils having thickness to chord ratio t/c greater than 0.15, leading edge stall occurs for airfoils having t/c of 0.09 to 0.15, and thin airfoil stall for airfoils having t/c less than 0.09.

The term dynamic stall refers to the unsteady separation and the stall phenomena of an airfoil oscillating into and out of stall. Figure 3 (from ref. 7), shows the flow field structure, as well as the normal force and pitching moment characteristics throughout an oscillation cycle of an airfoil during dynamic stall for an NACA 0012 airfoil. The predominant feature of dynamic stall (ref. 7), is the shedding of a strong vortex like disturbance from the leading edge region, which alters the chord wise pressure distribution. This vortex moves down stream over the upper surface of the airfoil at about 35 to 40 percent of free stream velocity. The unsteady aerodynamic forces due to the passage of this vorticity produce a lift and nose down moment, with values much greater than the corresponding static stall loads. The magnitude of the increase depends on the strength of the vortex and its distance from the surface. The formation and movement of the vortex depends on the airfoil shape,

angle of attack and the rate of angle of attack. The distance of the vortex from the airfoil depends on the rate of angle of attack and the instantaneous angle of attack. As the vortex leaves the trailing edge, a peak negative pitching moment is obtained. The airfoil then remains stalled until the angle of attack drops sufficiently for reattachment of the flow to occur.

It can also be seen that airfoils during dynamic stall exhibit large hysteresis loops in both lift and pitching moment curves when viewed as a function of angle of attack. This means that an airfoil with positive $\dot{\alpha}$ stalls at an angle α greater than the section static stall angle, α_{ss}, known as stall delay, while the stall recovery during negative $\dot{\alpha}$ occurs at an angle less than α_{ss}. It can also be observed that the pitching moment coefficient shows loops representing contributions to negative damping (clock-wise loops) and positive damping (counter clock-wise loops), and a net negative damping may lead to divergent oscillations. It is to be noted that for oscillations that occur wholly below or wholly within stall, there is always positive damping. Only for oscillations about a mean angle of attack near static stall can the net pitch damping become negative.

In summary, dynamic stall begins at an angle of attack greater than the static stall angle, followed by the shedding of vorticity from the leading and trailing edges. As the airfoil oscillates in and out of stall, the dynamic forces and moments show hysteresis and can attain values that are far greater than their static counterparts. The dynamic stall phenomenon and its effects vary depending on the airfoil shape, reduced frequency, mean angle and amplitude of oscillation, Mach number, Reynold's number, type of airfoil motion, sweep, and three-dimensional flow effects.

An important difference between stall flutter and classical flutter is in the character of flow. Stall flutter occurs with partial (light dynamic stall) or complete (deep dynamic stall) breakaway of the flow from the airfoil during at least part of every cycle of oscillation. This is in contrast to classical flutter, where the flow is attached to airfoil at all times. The essential feature of stall flutter is the nonlinear aerodynamic reaction to the motion of the airfoil. This nonlinear nature allows, in principle, the prediction of the final equilibrium amplitude of vibration (a limit cycle). This is different from classical flutter where only the stability boundary is usually determined. In short, stall flutter refers to a self-excited and self-sustained vibration in a periodically separated flow condition. Stall flutter also differs from classical flutter in that the torsional and bending frequencies are not necessarily close together even though both modes contribute to the stall flutter.

It has also been observed in stall flutter (ref. 8) that (1) there is a sharp drop in critical flutter speed, (2) the flutter frequency rises towards the torsional frequency, (3) the motion is predominantly torsion (single degree of freedom flutter), and (4) the stall flutter speed reaches a minimum and rises until the flow is completely stalled.

DYNAMIC STALL MODELING

The complexity in modeling stalling is due to the following reasons: (1) flow separation and turbulence effects during part of the cycle of oscillation; (2) a new variable, the mean angle of attack α_0, is introduced into

the determination of aerodynamic derivatives and automatically requires consideration of the effects of Reynold's number and airfoil shape; (3) the aerodynamic derivatives can no longer be simply superimposed (as in classical flutter) i.e., the aerodynamic results of a pitching motion cannot be separated from those of a simultaneous translatory motion; and (4) rate of angle of attack effects must be included in the analysis.

Earlier work on unsteady stalled flow has been either wholly experimental or consisted of empirical and semi-empirical modifications to classical flutter theory. These earlier studies have been based on the hypothesis that the decrease in flutter speed may be due to a decrease in aerodynamic torsional damping. Halfman, et al., (ref. 8) reviewed these methods and presented experimental data for lift and pitching moment in pure pitch, and in pure plunge. Sisto (ref. 9) presented a nonlinear mechanics approach to the problem of stall flutter, and verified his predictions with experiments for both isolated and cascade of blades. Schnittger (ref. 10), used data of Halfman et al. to investigate stall flutter in compressors and found that cascade effects have a suppressing effect on stall. Amer and La Forge (ref. 11) developed a procedure for calculating blade bending moments, torsion moments, negative aerodynamic damping, and the lift hysteresis during stall using Halfman, et al. experimental data. Baker (ref. 1) conducted experiments to measure the stall flutter speeds of thin wings representative of propeller blades. Rainey (ref. 12) measured aerodynamic damping to investigate stall flutter. Ham (ref. 13) conducted experiments to investigate stall flutter of helicopter blades. Carta (ref. 14) used an energy principle to calculate aerodynamic damping, and used Halfman et al. data at high angle of incidence for turbojet engines.

Recent research on dynamic stall followed two approaches, one theoretical (refs. 15 to 32), and the other based on experimental data, references 33 to 41. These research efforts on dynamic stall are summarized in references 42 to 47. The flow elements to be included in dynamic stall modeling are discussed in reference 48. Reference 47 tabulated the dynamic stall prediction methods according to the technique used in the formulation, and roughly graded most of the models according to the salient features of each model. An updated version of the table is presented in table I, from which the strengths and weaknesses of the models can be seen more readily.

The theoretical approaches are the Navier-Stokes methods, the discrete vortex methods, and coupled viscous-inviscid methods (zonal methods). Navier-Stokes methods (refs. 15 to 17) attempt to solve the relevant equations in their fundamental form by numerical techniques. The discrete vortex approach (refs. 18 to 24) normally ignores the viscous terms in the basic equations and assumes potential flow without the boundary layer. The viscous nature of the flow is modeled or taken into account, by the generation and subsequent induced transport of discrete combined vortices. The manner and location of their generation is normally obtained empirically or via appropriate boundary layer calculations. In the zonal methods (refs. 24 to 32) the various regions of flow, viscous, nonviscous, and transition regions, are modeled separately. In the numerical implementation of the model, the regions interact in an iterative manner. These theoretical models require a lot of computer time and are limited by the assumptions and restrictions of the formulation. So they are not suitable in a routine aeroelastic analysis.

Semi-empirical methods (refs. 33 to 41) based on experiments attempt to simulate the gross features of stall. They have gained much interest for the

following reasons: (1) they attempt to use static data with a dynamic correction. This is advantageous because static data can be easily generated and automatically includes the effects of Reynold's number, Mach number, and airfoil shape. (2) They take less computer time so they can be used in a routine aeroelastic analysis.

In the published literature there are four types of models for dynamic stall based on experimental data (semi-empirical). The first (ref. 33) is to use measured data tabulated in a three-dimensional array (angle of attack, reduced pitch rate, reduced pitch acceleration) with an appropriate correction for local Mach number. This requires a large amount of data storage for each airfoil, frequency of oscillation and the associated interpolation. The second (refs. 34 and 35) is to utilize a corrected angle of attack when the angle exceeds the static stall angle. This correction is a function of the rate of change of angle of attack.* The third (refs. 37 and 38) is to reduce the large volume of data obtained from experiments to compact expressions (synthesization). The fourth (ref. 39) is to describe the lift and moment coefficients in terms of ordinary differential equations (ONERA model). The last two models attempt to fit the experimental data by way of equations. It should be noted that in the first two models the time history of the motion is not taken into account.

The empirical parameters used in the semi-empirical models referred above are usually obtained from airfoils oscillating in pitch about quarter-chord. However, an arbitrary motion includes both pitch and plunge motions. So stall modeling should include separate $\dot{h}$ and $\ddot{h}$ terms in the identification of the empirical parameters. This would seem to require experiments that allow for plunge as well as pitch motions. But, it would certainly be convenient if only dynamic-pitch experiments were needed and the plunge effects could be derived from them by other means. Many of the existing dynamic stall modeling methods do not take into account this distinction. Reference 49 maintains that the equivalence between pitch and plunge is not valid since the way the stall cell forms and propagates is different in pitch and plunge. However, tests have shown that the equivalence between pitch and plunge is reasonable in light stall but not in deep stall. For more discussion on the equivalence of pitch and plunge see references 50 and 51. In the semi-empirical models, mentioned above, the ONERA model attempts to take this distinction into account.

In the following the last three semi-empirical models, which are designated as A, B, and C, are described. These methods are selected on the basis of their availability and easy implementation. Equations are presented to calculate lift and pitching moment coefficients. Equations similar to those given for pitching moment coefficient can be used to calculate coefficient of drag. It is to be noted when calculating the resultant velocity on the airfoil that the present study is restricted to nonrotating structural models, hence the resultant velocity is same as the free stream velocity.

---

*The MIl model of reference 36, corrects the angle of attack as a function of rate of angle of attack, but idealizes the loading due to vortex as an impact load at the instant of stall occurrence. The magnitude of this impact loading is obtained from experiments.

MODEL A - CORRECTED ANGLE OF ATTACK APPROACH

This model is presented in references 34 and 35. In this model, the actual angle of attack, α, is corrected to obtain an effective angle of attack α_E. Then, the coefficients c_ℓ and $c_{mc/4}$, which are functions of Mach number, are obtained from static airfoil data. The correction to the angle of attack is a function of rate of angle of attack and is based on oscillating airfoil test data.

The relation between the actual and the effective angle of attack is given in terms of an incremental dynamic stall angle, $\Delta\alpha_{DS}$, as

$$\alpha_E = \alpha - K_1 \Delta\alpha_{DS} \tag{1}$$

Then an empirical relation is established from experiments between $\Delta\alpha_{DS}$ and the rate of angle of attack as,

$$\Delta\alpha_{DS} = \gamma\sqrt{\left|\frac{\dot{\alpha}c}{2V}\right|} = \gamma\sqrt{|A|} \tag{2}$$

Here V is the resultant velocity, c is the chord of the airfoil, $\dot{\alpha}$ is the rate of angle of attack, A is the nondimensional rate of angle of attack, the function γ has to be determined empirically from oscillating airfoil test data, and K_1 is given by

$$K_1 = 3/4 + 1/4\ \text{sign}(\dot{\alpha}) \tag{3}$$

The function γ is a function of Mach number, airfoil maximum thickness to chord ratio and has different values for lift and moment. This indicates that the influence of γ is not the same for both lift stall and moment stall.

From equation (2), it can be seen that γ is the slope of the straight line representing the variation of $\Delta\alpha_{DS}$ with $\sqrt{|A|}$. The slope is constant for thicker airfoils. However, for thin airfoils, experimental data reveal that there are two slopes γ_1 and γ_2, depending on the values of $\sqrt{|A|}$. The value of $\sqrt{|A|}$ at which the slope changes is designated as $\sqrt{|A|}_{Break}$. The definitions of γ_1, γ_2, $\Delta\alpha_{DS}$, and $\sqrt{|A|}$ are schematically shown in figure 4. The values of γ, for both lift stall and moment stall are listed below:

Lift Stall

$$\gamma_{2L} = 1.4 - 6.0\ (0.06 - t/c), \qquad \text{If Mach No.} < 0.4 + 5.0\ (0.06 - t/c)$$

$$\gamma_{2L} = 0. \qquad \text{If Mach No.} > 0.9 + 2.5\ (0.06 - t/c)$$

$$\gamma_{1L} = 0.5 \tag{4}$$

Moment Stall

$$\gamma_{2M} = 1.0 - 2.5\ (.06 - t/c), \qquad \text{If Mach No.} < 0.2$$

$$\gamma_{2M} = 0. \qquad \text{If Mach No.} > 0.7 + 2.5\ (.06 - t/c)$$

$$\gamma_{1M} = 0.0 \tag{5}$$

where subscripts L and M denote lift and moment respectively. It is to be noted that in the above expressions, the effect of Mach number is included in the definition of γ_1 and γ_2. The variation of γ_2 with Mach number is schematically shown in figure 4. Also based on experimental data, $\sqrt{|A|}_{Break}$ is expressed in terms of t/c as

$$\sqrt{|A|}_{Break} = 0.06 + 1.5\ (0.06 - t/c) \tag{6}$$

The next step is to express $\Delta\alpha_{DS}$ in terms of γ_1, γ_2, and $\sqrt{|A|}$.

$$\Delta\alpha_{DS} = (\gamma_{1(L,M)}\ \sqrt{|A|})\ (\text{sign}\ \dot{\alpha}) \quad \text{if} \quad \sqrt{|A|} < \sqrt{|A|}_{Break} \tag{7}$$

$$\Delta\alpha_{DS} = \left(\gamma_{1(L,M)}\ \sqrt{|A|}_{Break} + \gamma_{2(L,M)}\ (\sqrt{|A|} - \sqrt{|A|}_{Break})\right)\text{sign}\ (\dot{\alpha})$$

$$\text{if} \quad \sqrt{|A|} > \sqrt{|A|}_{Break} \tag{8}$$

This formulation has the effect of reducing the angle of attack for positive $\dot{\alpha}$, and of increasing the angle of attack for negative $\dot{\alpha}$. The final lift and moment coefficients are calculated as

$$C_\ell = \left(\frac{C_\ell(\alpha_E)}{\alpha_{E,L} - \alpha_{C_\ell = 0}}\right)\alpha \tag{9}$$

$$C_{mc/4} = C_m(\alpha_{E,M}) \tag{10}$$

where $\alpha_{C_\ell = 0}$ is the angle of attack for zero lift.

It should be noted that in this formulation the effects of Mach number and thickness to chord ratio are explicitly included. This will be useful in the application of this model directly to advanced turboprop blades, which are very thin, operate at different Mach numbers along the radius, and have a varying thickness to chord ratio along the radius. It should be noted that above formulation is used only when the actual angle of attack is above the static stall angle. This implies that after separation of the flow, the reattachment is assumed at static stall angle. Reference 38 observed that this may not reproduce the pitching moment loop correctly, thereby affecting the aerodynamic damping calculations.

MODEL B - SYNTHESIS PROCEDURE

Reference 38 presents a synthesized approach to dynamic stall modeling. The synthesized data essentially consist of semi-empirically obtained analytical expressions representing qualitative approximations to the various observed physical features associated with the dynamic stall of airfoils. The model adequately accounts for the effects of formation and streamwise travel of the dynamic stall vortex. The process involves curve-fitting analytic expressions to the test loop data with the objective of determining the unknown parameters or coefficients embedded in the analytical expressions.

Three dynamic parameters are defined to predict the dynamic stall events: (1) the instantaneous angle of attack, α; (2) the nondimensional rate of angle of attack, A; and (3) a decay parameter, α_W, which accounts for the time history effects of the change in α, and is based on the Wagner function. The data on which this synthesis procedure is based accounts for some effects of airfoil shape, Mach number, and Reynold's number. In the following, the decay parameter, α_W is defined, then three stages of dynamic stall are identified and expressed in terms of the empirical parameters obtained from the synthesis procedure. The relations for unsteady lift and moment based on the above parameters are presented.

Definition of α_W

For a two-dimensional airfoil going through an arbitrary change in angle of attack, one can describe an instantaneous effective angle of attack, α_E, by using Duhamel's integral (ref. 40),

$$\alpha_E(s) = \alpha(0)\phi_c(s,M) + \int_0^s \frac{d\alpha}{d\sigma}\,\phi_c(s-\sigma,M)\,d\sigma \qquad (11)$$

where $\alpha(0)$ corresponds to the initial angle of attack, M represents Mach number, ϕ_C (s,M) (Wagner function) is the response to a step change in α, and s is the nondimensional time given by

$$s = 2V\ t/c \qquad (12)$$

The decay parameter is given by

$$\alpha_W = \alpha(s) - \alpha_E(s) \qquad (13)$$

The decay parameter, α_W, is the difference between the instantaneous angle, α (s), and the effective angle α_E, and, therefore, acounts for the time history effects of the change in α. The effect of compressibility is also incorporated in the definition of α_W, by defining

$$\phi_C\ (s,M) = 1. - 0.165\ e^{-0.0455\ (1-M^2)} - 0.335\ e^{-0.35\ (1-M^2)} \Big/ \sqrt{(1. - M^2)} \qquad (14)$$

The calculation of A, and α_W for sinusoidal motion and arbitrary motion are given in the latter sections.

Prediction of Dynamic Stall Events

In the published literature, three stages of dynamic stall are defined: (1) the onset of stall, which gives the angle at which stall starts (see fig. 3); (2) the vortex at the trailing edge, which gives the time (nondimensional) taken for the vortex to travel to the trailing edge; and (3) the reattachment, the angle at which the flow reattaches to the airfoil. In the present model these three stages are related empirically by the nondimensional rate of angle of attack, A, the decay parameter, α_w, and the static stall angle, α_{ss}. The values of A, α_w, and α_{ss} correspond to the values at the instant of moment stall, since moment stall occurs prior to lift stall.

Onset of stall: The angle of attack at which the stall begins is given by

$$\alpha_{Dm} = (1. + \varepsilon + C_{Am}A_m + C_{wm}\alpha_{wm})\,\alpha_{ss} \tag{16}$$

where subscript m refers to values at the point of moment stall and the empirical parameters ε, C_{Am}, and C_{wm} are obtained from curve fitted experimental data.

Vortex at the trailing edge: After the occurrence of moment stall, there is a significant increase in negative pitching moment due to the travel of the stall vortex. The maximum negative pitching moment occurs when the vortex is near the trailing edge of the airfoil. The time at which the vortex leaves the trailing edge is given by

$$s_{mt} = 1.0/(C_{At}A_m + C_{\alpha t}\alpha_{Dm}) \tag{17}$$

where s_{mt} is the total nondimensional time for the vortex to travel from the leading edge to the trailing edge, and the empirical parameters C_{At} and $C_{\alpha t}$ are obtained from experiments.

Reattachment: For Mach numbers < 0.4, the reattachment occurs at an angle α_{RE} which is less than the static stall angle. At higher Mach numbers, α_{RE} can be greater than the static stall angle α_{ss}.

$$\alpha_{RE} = (1 - \varepsilon + C_{AR}A_m + C_{wR}\alpha_{wm})\,\alpha_{ss} \tag{18}$$

The empirical parameters C_{AR} and C_{wR} are curve fitted for a given airfoil from experiments.

In summary, there are seven empirical parameters to predict the dynamic stall events and they depend on Mach number, Reynold's number, sweep angle and airfoil shape.

Now the unsteady lift and moment coefficients, including dynamic stall effects, are expressed in terms of additional empirical parameters and are given below.

Unsteady Lift Coefficient

$$c_\ell = C_{LU} = C_{LS}\,(\alpha - \Delta\alpha_1 - \Delta\alpha_2) + a_{o\ell}\Delta\alpha_1 + \Delta C_{L1} + \Delta C_{L2} \tag{18a}$$

$$\Delta\alpha_1 = (P_1 A + P_2 \alpha_w + P_3)\, \alpha_{ss} \tag{18b}$$

$$\Delta\alpha_2 = \delta_2 \alpha_{ss} \tag{18c}$$

$$\Delta C_{L1} = Q_1 A + Q_2 \alpha_w + Q_3 (\alpha/\alpha_{ss}) + Q_4 (\alpha/\alpha_{ss})^2 \tag{18d}$$

$$\Delta C_{L2} = Q_5 \delta_1 + Q_6 \Delta\alpha_2 + Q_7 (\alpha_{Dm})^2 \left[\frac{1 - e^{-(\beta_1 s_m)^3}}{(\beta_1 s_m)^2} \right] \tag{18e}$$

$$s_m = \frac{2V (t - t_{dm})}{c} \tag{18f}$$

$$\delta_1 \begin{cases} = 0 & \alpha \leq \alpha_{ss} \\ = \dfrac{\alpha}{\alpha_{ss}} - 1 & \alpha_{ss} < \alpha \leq \alpha_{Dm} \\ = \left[\dfrac{\alpha_{Dm}}{\alpha_{ss}} - 1 \right] \left[1 - \left(\dfrac{s_m}{s_{mt}} \right)^2 \right] & 0 \leq s_m \leq s_{mt} \\ = 0 & s_m > s_{mt} \end{cases}$$

$$\delta_2 \begin{cases} = 0 & \alpha \leq \alpha_{ss} \\ = \dfrac{\alpha}{\alpha_{ss}} - 1 & \alpha_{ss} \leq \alpha \leq \alpha_{Dm} \\ = \dfrac{\alpha_{Dm}}{\alpha_{ss}} - 1 & 0 \leq s_m \leq s_{mt} \\ = \left[\dfrac{\alpha_{Dm}}{\alpha_{ss}} - 1 \right] \left[\dfrac{\alpha - \alpha_{RE}}{\alpha_{TE} - \alpha_{RE}} \right] & \alpha_{RE} < \alpha < \alpha_{TE} \\ = 0 & \alpha < \alpha_{RE} \end{cases} \tag{18g}$$

where δ_1 and δ_2 depend on onset of stall and reattachment.

In equation (18a), $a_{o\ell}$ is the conventional static lift curve slope. The shift in angle of attack, $\Delta\alpha_1$ and $\Delta\alpha_2$, are associated respectively with the unsteady effects below stall and with the occurrence of dynamic stall and reattachment. ΔC_{L1} represents the unsteady effects over static lift for unstalled airfoils, and ΔC_{L2} represents the effects associated with dynamic stall. Equation (18a) expresses the synthesized unsteady coefficient as a sum of static lift coefficient, C_{LS}, at some shifted angle ($\alpha - \Delta\alpha_1 \Delta\alpha_2$) plus an

increment lift coefficient ($\Delta C_{L1} + \Delta C_{L2}$). For unstalled cases $\Delta\alpha_2$ and ΔC_{L2} are zero. Also $\beta_1 = 0.18$, s_m is time measured from the instant of the occurrence of dynamic moment stall. The parameters P_1 through P_3 and Q_1 through Q_7 are determined empirically by means of least squares curve fitting of equation (18a) with the test data.

Unsteady Moment Coefficient

$$C_{mc/4} = C_{MU} = C_{MS}(\alpha - \Delta\alpha_2) + a_{om}\Delta\alpha_2 + \Delta C_m \tag{19a}$$

$$\Delta C_m = \eta_1 A + \eta_2 \alpha_w + \eta_3 \left(\frac{\alpha}{\alpha_{ss}}\right) + \eta_4 |\alpha_w| + \eta_5 \delta_1 + \eta_6 \Delta\alpha_2 + \eta_7 \alpha_{Dm} A_{Dm} s_m \tag{19b}$$

In equation (19a), a_{om} is the static moment at zero angle of attack, normally zero, and C_{MS} is the static moment coefficient about quarter chord. The parameters η_1 through η_7 are determined by least square curve fitting of the test data. For unstalled airfoils, the last three terms are zero.

It should be noted that (1) the delay, the time from the onset of static stall to actual stall, is taken into account by calculating the actual dynamic stall angle from the curve fitted experimental data, (2) the difference in pitching and plunging motion is not taken into account explicitly. The total angle of attack and its derivative are used in the formulation, and (3) vortex formation and its effects are accounted for.

MODEL C - ONERA MODEL

The ONERA model (ref. 39) describes the lift and moment coefficients in terms of ordinary differential equations. The equations are of first order in the linear flow regime (attached flow), and they are of third order in the nonlinear regime (separated flow). the third order equation simulates the pseudo inertial, pseudo damping, and pseudo elastic forces of a fluid oscillator. The parameters (six for lift, and five for moment) in the differential equations are identified, as functions of angle of attack, by parameter identification of test data. These tests are conducted about each mean angle of attack at various reduced frequencies at small amplitude ($\approx 1°$) of oscillation. They showed good correlation for angles of attack up to 23°. Reynold's number and Mach number effects are included implicitly from a static airfoil data base. It should be noted that a differential equation automatically accounts for the time-history effects.

The model consists of three equations that relate the lift coefficient of an airfoil to its angle of attack. They are:

$$\overset{*}{C}_{L1} + \lambda C_{L1} = \lambda C_{L\ell} + \lambda s\overset{*}{\theta} + \sigma\overset{*}{\alpha} + s\overset{**}{\theta} \tag{20a}$$

$$\overset{**}{C}_{L2} + a\overset{*}{C}_{L2} + rC_{L2} = -(r\,\Delta C_L + E\overset{*}{\alpha}) \tag{20b}$$

$$c_\ell = C_{L1} + C_{L2}; \qquad \alpha = \theta + \frac{\dot{h}}{b} \tag{20c}$$

where C_{L1} and C_{L2} are the lift coefficients in the linear and nonlinear regions of angle of attack (below and above static stall angle respectively), α is the total aerodynamic angle of attack of the airfoil, θ is the angle of attack due to pitching motion, and $\dot{h}/b$ is the angle of attack due to plunging motion. $C_{L\ell}$ is the static lift coefficient in the linear region of angle of attack. ΔC_L is the difference between the extended linear lift curve ($C_{L\ell} = a_{0\ell}\alpha$) and the actual static lift curve (C_{LS}). c_ℓ is the resulting total lift coefficient as shown in figure 5.

Similarly, the moment coefficient can be expressed as a first order differential equation for angles below static stall angle with an additional second order differential equation for angles above static stall angle. However, the first order differential equation is not necessary for moment coefficient since the Theodorsen function $C(k)$ does not appear in equation for moment coefficient in Theodorsen's moment equation for a flat plate, reference 52, equation (5-312). Therefore the equations for moment coefficient are given as

$$C_{M1} = C_{M\ell} + s\dot{\theta} + \sigma\dot{\alpha} + s\ddot{\theta} \tag{20d}$$

$$\ddot{C}_{M2} + a\dot{C}_{M2} + rC_{M2} = -(r\,\Delta C_M + E\dot{\alpha}) \tag{20e}$$

$$c_{mc/4} = C_{M1} + C_{M2} \tag{20f}$$

where C_{M1} and C_{M2} are the moment coefficients in the linear and nonlinear regions of angle of attack. $C_{M\ell}$ is the static moment coefficient in the linear region. ΔC_M is the difference between the extended linear curve and the actual static curve as shown in figure 5. $c_{mc/4}$ is the resulting total moment coefficient.

In equations (20a) to (20e), the $(\dot{})$, $(\ddot{})$ operators represent derivatives with respect to nondimensional time, $\tau = V\,t/b$. The values of the parameters, λ, s, a, σ, r, E are different for lift and moment coefficients, and are obtained from wind tunnel tests. However, their general behavior can be identified and is presented below.

For an airfoil with a fixed Reynold's number, and Mach number, the parameters λ, s, a, σ, r, E are functions of the blade angle of attack only, and must be determined from wind tunnel test data of the corresponding airfoils by parameter identification. The parameter, λ, is the time-delay parameter associated with the lift deficiency function. It provides for changes in magnitude and phase of the lift. The parameter s is the apparent mass term. The parameters in equations (20b) and (20e) are associated with the stall phenomenon. In particular, a is a damping parameter; r is the frequency of the stall response, and E is a phase shift parameter associated with the stall response. The parameters defining the differential equations showed a remarkably common behavior with several airfoils, that is they have shown approximately the same values for r, a, E, σ for each airfoil, and same dependence on ΔC_L. The parameter r happens to be the same for lift and for moment. This means that the resonance frequency is in fact a property of the flow

which manifests itself in every type of force. The static values (C_{LS}, C_{MS}) can be approximated by polynomials. The static curves are very sensitive to airfoil shape and conditions of flow, but the unsteady characteristics are not.

It should be noted that the stall delay time, the time from the instant the angle of attack exceeds the static stall angle to the occurrence of actual stall, is introduced explicitly while solving the equations. This is done by keeping the right-hand side of equations (20b) and (20e) equal to zero until the static stall angle is reached and the delay time is met. This delay time (in terms of reduced time), based on experimental data, is taken as 10 for lift and 5.8 for moment (see ref. 40). The effects of pitch and plunging motion are distinguished by separating the terms that multiply the total angle of attack (pitch + plunge) and that multiply the pitch rate terms. This is in contrast to model A and model B, where such distinction was not made. However, it should be noted that in the ONERA model, the system dimension increases with number of integration points (3 for lift and 2 for moment), and it can be used in a linearized stability analysis.

In reference 53, the equations (20a) to (20e) are used to obtain the dynamic response of a typical section helicopter blade, and in reference 54 to an entire helicopter blade. It should be noted that this type of modeling, expressing aerodynamic force in the form of differential equations has been attempted in reference 55. In particular reference 56 has used it in the dynamic stall analysis of helicopter blades.

A flow chart of the three dynamic stall models is given in figure 6.

GOVERNING AEROELASTIC EQUATIONS OF MOTION

This section presents the governing equations used in the aeroelastic study conducted with the three dynamic stall models described earlier. Three simple structural models are considered.

1. Calculation of lift and moment coefficients for airfoils oscillating sinusoidally in pitch about quarter chord. This study will show the degree of correlation with published results.

2. A typical section model having pitching and plunging motion.

3. A plate model having pitching and plunging motion.

The flat plate case simulates the case of an advanced turboprop while reducing the complexity in the structural modeling. When the aeroelastic equations are formulated in terms of normal modes, for example as in reference 2, the structural modeling is identical with that of flat plate. For the aerodynamic force calculations, the dynamic stall models require as input the angle of attack and its derivatives at each section along the radius. This can be easily implemented in the flat plate model by including the rotational effects in the calculation of angle of attack and its derivatives. Hence a flat plate case is a natural example to start with and to extend to the advanced turboprop.

Airfoils Oscillating Sinusoidally in Pitch About Quarter Chord

For stall models A and C, the angle of attack and its time derivatives are given by

$$\begin{aligned} \alpha &= \alpha_0 + \bar{\alpha} \sin \omega t \\ \dot{\alpha} &= \omega \bar{\alpha} \cos \omega t \\ \ddot{\alpha} &= -\omega^2 \bar{\alpha} \sin \omega t \end{aligned} \tag{21}$$

where α is the instantaneous angle of attack, α_0, mean angle of attack, $\bar{\alpha}$ is amplitude of oscillation, and ω is the frequency of oscillation. A time delay of 10 for lift and 5.8 for moment is used in model C, based on the study of reference 40.

For stall model B, the angle of attack, α, nondimensional time derivative of angle of attack, A, and the decay parameter, α_W, required in the calculation of the effective angle of attack are given by

$$\alpha = \alpha_0 + \bar{\alpha} \sin (\omega t) \tag{22}$$

$$= \alpha_0 + \bar{\alpha} \sin (ks) \tag{23}$$

$$A = k \bar{\alpha} \cos (ks) \tag{24}$$

$$\alpha_W = A\gamma_1 (k,M) + (\alpha - \alpha_0)\, \gamma_2(k,M) \tag{25}$$

where $k = \omega b/V$, $s = Vt/b$ and

$$\gamma_1(k,M) = \frac{0.165\,(1-M^2)\,(0.0455)}{k^2 + (1-M^2)^2\,(0.0455)^2} + \frac{0.335\,(1-M^2)\,(0.3)}{k^2 + (1-M^2)^2\,0.3^2} \tag{26}$$

$$\gamma_2(k,M) = \frac{0.165\,k^2}{k^2 + (1-M^2)^2\,(0.0455)^2} + \frac{0.335\,k^2}{k^2 + (1-M^2)^2\,0.3^2} \tag{27}$$

For each time step n, the angle of attack, A and α_W are calculated. The angle of attack is compared with the static stall angle. If this angle is above the static stall angle, the lift and moment coefficients are obtained from corresponding equations of the three dynamic stall models. Then the normal force coefficient, C_N, is given by $c_\ell \cos(\alpha)$. It should be noted that in contrast to models A and B, model C requires integration of differential equations.

A Typical Section Model

The typical section is a representative section, usually taken at 75 percent span. Figure 7, shows a typical section oscillating in pitch and plunge. The plunge motion h is positive downwards, and the pitch motion α is positive nose up. The equations of motion can be written as

$$m\ddot{h} + S\ddot{\alpha} + C_h\dot{h} + K_h h = Q_h \tag{28}$$

$$S\ddot{h} + I_\alpha\ddot{\alpha} + C_\alpha\dot{\alpha} + K_\alpha\alpha = Q_\alpha \tag{29}$$

where m is the mass, S is static balance, K_h is the plunge spring coefficient, K_α is the pitching spring coefficient, C_h and C_α are the mechanical damping in plunge and pitch respectively, Q_h and Q_α are the force and moment on the airfoil.

Letting $\bar{t} = \omega t$, and $\xi = h/b$, the equations can be written as

$$\xi'' + \bar{x}_\alpha\alpha'' + \zeta_h\xi' + \left(\frac{\omega_h}{\omega}\right)^2 \xi = \frac{Q_h}{mb\omega^2} \tag{30}$$

$$\bar{x}_\alpha\xi'' + r_\alpha^2\alpha'' + \zeta_\alpha\alpha' + r_\alpha^2\left(\frac{\omega_\alpha}{\omega}\right)^2 \alpha = \frac{Q_\alpha}{mb^2\omega^2} \tag{31}$$

With zero mechanical damping, and expressing Q_h and Q_α in terms of normal force, C_N, and moment coefficients, c_m, respectively, equations (30) and 31 can be written as

$$[M]\begin{Bmatrix}\xi\\ \alpha\end{Bmatrix}'' + \frac{1}{(U^*k)^2}[K]\begin{Bmatrix}\xi\\ \alpha\end{Bmatrix} = \frac{1}{\pi\mu k^2}\begin{Bmatrix}-C_N\\ c_m\end{Bmatrix} \tag{32}$$

where $k = \omega b/V$, $U^* = V/b\omega_\alpha$, $\mu = m/\pi\rho b^2$.

The elements of $[M]$ and $[K]$ are

$$M_{11} = 1.0, \qquad M_{12} = M_{21} = \bar{x}_\alpha, \qquad M_{22} = r_\alpha^2$$

$$k_{11} = \left(\frac{\omega_h}{\omega_\alpha}\right)^2, \qquad k_{12} = k_{21} = 0, \qquad k_{22} = r_\alpha^2$$

where $\bar{x}_\alpha$ is the static unbalance, r_α is radius of gyration, ω_h, ω_α are uncoupled bending and torsion frequencies, ρ is the density of air, b is semi-chord, m is the mass per unit length, μ is the mass ratio, V is the resultant velocity, and ω is reference frequency.

In the previous section, the angle of attack and its derivatives were given explicitly for sinusoidal oscillations. However, a structure performs a more general motion. Therefore, it is required to calculate the angle of attack (α), the nondimensional time rate (A) and the decay parameter (α_w), for an arbitrary motion. This is given below.

At any time step n, the velocities tangential and perpendicular to the leading edge are given by (see fig. 7)

$$Up = \dot{h} + x\dot{\alpha} + V\sin(\alpha_0 + \alpha) \tag{33}$$

$$U_T = V \cos (\alpha_0 + \alpha) \tag{34}$$

from which the instantaneous angle of attack is given by

$$\alpha_n = \arctan \left(\frac{U_P}{U_T} \right) \tag{35a}$$

With this instantaneous angle of attack, the parameter A and α_w are determined by using the following equations:

$$(A)_n = \frac{(d\alpha)}{(ds)_n} = \frac{(1.5\alpha_n - 2\alpha_{n-1} + 0.5\alpha_{n-2})}{(\Delta s)_n} \tag{35b}$$

using the backward difference scheme, and

$$(\alpha_w)_n = X_n + Y_n \tag{35c}$$

where

$$X_n = X_{n-1} \, e^{-0.0455 (1-M^2) (\Delta s)_n} + 0.165 (\alpha_n - \alpha_{n-1})$$

$$Y_n = Y_{n-1} \, e^{-0.3 (1-M^2) (\Delta s)_n} + 0.335 (\alpha_n - \alpha_{n-1}) \tag{35d}$$

$$(\Delta s)_n = 2 U_n \frac{t}{c}$$

where c is the chord, U_n is the velocity normal to the leading edge at time step n, and subscripts n, $(n-1)$, etc., indicate the values at the n, $(n-1)$ th step in a step-by-step integration method.

For these aerodynamic parameters, α, A, α_w, the lift and moment coefficients (about quarter chord) are calculated from the dynamic stall models A and B described earlier. Then the aerodynamic normal force and moment coefficients about the elastic axis are given by

$$C_N = c_\ell \cos \alpha \tag{36}$$

$$c_m = c_{mc/4} + \frac{C_N}{2} (a_h + 0.5) \tag{37}$$

where $c_{mc/4}$ is the moment coefficient calculated about quarter chord point. In the case of dynamic stall model C, the stall parameters appearing in equations (20a) to (20e) are calculated using the above aerodynamic parameters, and the differential equations (20a) to (20e) are integrated along with the structural equations given in equation (32). A state vector form of this combined structural/stall model is given in section A.1 of appendix A.

Plate Model

The governing equations of motion are formulated in terms of normal modes of a cantilevered plate. The nonrotating normal modes of the plate are obtained from a NASTRAN analysis. Since any general vibratory motion of the plate can be expressed in terms of translation of some reference axis and rotation about this reference axis, the plunge and pitch motions are expressed about a reference axis. If $h(y)$ is the bending deflection of the reference axis at station y, when the blade is vibrating in the ith normal (coupled) mode, and $\alpha(y)$ is the rotation about the reference axis, the displacement at station y can be expressed as a superposition of the contributions of the various normal modes as

$$h = \sum h_i \, q_i(t)$$
$$\alpha = \sum \alpha_i \, q_i(t) \tag{38}$$

where $q_i(t)$ is the generalized coordinate, which is a function of time. The amplitude $q_i(t)$ expresses how much of each normal mode is introduced into the general vibratory motion. The kinetic energy dT of an element dY is

$$dT = \frac{1}{2} [m(y)\dot{h}(y,t)^2 + I_\alpha(y)\dot{\alpha}(y,t)^2 + S(y)\dot{h}(y,t)\dot{\alpha}(y,t)] \tag{39}$$

Substituting for h and α and integrating over the span the total kinetic energy is given by

$$T = \frac{1}{2}\sum m_i \, \dot{q}_i^2 \tag{40}$$

where

$$m_i = \int (mh_i^2 + I_\alpha \alpha_i^2 + 2 S h_i \alpha_i) \, dy \tag{41}$$

with the normality condition

$$\int [mh_i h_j + I_\alpha \alpha_i \alpha_j + S(h_i \alpha_j + \alpha_i h_j)] \, dy = 0 \tag{42}$$

The potential energy is

$$U = \frac{1}{2}\sum m_i \omega_i^2 \, q_i^2 \tag{43}$$

where ω_i is the circular frequency of vibration in the ith normal mode. Then the governing equations of motion can be written as

$$m_i \ddot{q}_i + m_i \omega_i^2 q_i = Q_i \tag{44}$$

where Q_i is the generalized force including aerodynamic forces.

Aerodynamic Velocity Expressions

In the present study, simple strip theory is used to calculate the blade velocities and forces. Therefore the plate is divided into a number of strips (segments). For a flat-plate with no pretwist, the velocities at each segment are given by the same expressions as for a typical section model. Therefore the angle of attack is given by equation (33), after expressing h and α motions in terms of normal modes. Then c_ℓ and $c_{mc/4}$ are calculated from any of the dynamic stall models described earlier. The lift and moment coefficients at this segment are given by equation (36), from which the actual lift and moment are calculated. Then the generalized force at segment, j, in ith mode is given by

$$f_{ij} = (h_i(y)L + \alpha_i(y)\, M)\, dl \tag{46}$$

where dl is the length of the segment, L and M are the lift and moment at jth segment, and $h_i(y)$ and $\alpha_i(y)$ are values of h and α at the center of the jth segment.

The total generalized force on the blade for ith mode is given by

$$Q_i = \sum_{j=1}^{N} f_{ij} \tag{47}$$

where N is the number of segments, the structure is divided into. The equations of motion are solved for this time step.

It should be noted that for stall model C, the lift and moment coefficients are given in the form of differential equations, and the combined structural/stall model has to be solved for each time step. For a plate (continuum) model, the number of equations in the combined structural/stall model depend not only on the number of normal modes used, but also on the number of segments into which the blade is divided. A state vector form of this combined structural/stall model for model C is given in section A.2 of appendix B.

RESULTS AND DISCUSSION

The numerical results of the study are presented in this section. The three aerodynamic stall models explained earlier are used for comparative studies. The results and discussion are performed for three simple structural models: (1) an isolated airfoil oscillating sinusoidally in pitch about quarter chord; (2) a typical section model performing pitching and plunging oscillations; and (3) a flat-plate model performing pitching and plunging oscillations. A computer program with these dynamic stall models and structural models has been developed and will be expanded to consider the aeroelastic response of advanced turboprops. The following results show the validity of the computer program and an assessment of the three dynamic stall models. The experimental data presented in this report was obtained from enlarged published plots.

In this study all the calculations are made for three airfoils, namely NACA 0012, NACA 0012 (MOD) and OA212, and for Mach numbers of 0.3 and 0.4, since the semi-empirical data is readily available for these Mach numbers. As

pointed out earlier, the dynamic stall effects vary with airfoil geometry and Mach number. However, the following comment can be made for stall at higher Mach numbers. The static stall angle decreases as the Mach number increases and the blade may stall earlier than at low Mach numbers. Experimental data of reference 56 showed that for Mach number equal to 0.6 there is shock-induced separation and stall. The dynamic data suggested that the formation of shock waves somehow inhibit the development of the vortex shedding process.

At this pint, a mention of the effects of other parameters on dynamic stall is in order. Experimental results of reference 7 indicated that, (1) increasing reduced frequency decreases the intensity of the dynamic stall vortex shedding and delays the formation and growth of the leading edge vortex, (2) cambering the leading edge tends to delay stall onset, (3) the higher the Reynold's number, the later the separation appears and develops, (4) sweep reduces dynamic stall effects, (5) the effect of decrease in thickness is similar to the effect of an increase in Mach number, and (6) cascades reduce dynamic stall effect. The dynamic stall effects also depend on mean angle and amplitude of oscillation.

It should be noted that when comparing with published results some quantitative differences may exist since the dynamic stall loads are sensitive to airfoil static data used. For completeness, the static data (c_ℓ and $c_{mc/4}$ versus α), and the dynamic stall data for the airfoils mentioned above are given in appendices B and C. When comparing results from model C with those obtained from model A and model B, it should be noted that model C involves integration of lift and moment equation simultaneously with structural equations.

Isolated Airfoil Oscillating in Pitch About Quarter Chord

Verification of the published results. - The intention here is to verify the published results and to check whether the dynamic stall models are correctly implemented in the computer program.

Stall model A: In reference 35, this model was applied to four airfoils, namely the V23010-1.58, NACA 0012(MOD), V13006-.7, and NACA 0006, and the theoretical and measured lift and moment coefficients were correlated. In the correlation, a variation in the mean angle of attack, amplitude of oscillation, Mach numbers, and reduced frequency was considered. The test data included forced pitch oscillations for the four airfoils and plunging oscillations for the V23010-1.58 airfoil. It was concluded that overall correlation between theory and test was good for the normal force coefficient and was acceptable for pitching moment coefficient.

To facilitate interpretation of analytical model A, the lift and moment coefficients are calculated herein and are shown in figures 8 and 9 along with the measured data. The NACA 0012(MOD) airfoil in pitching motion at 0.4 Mach number is considered. Figure 8 presents the plots for a mean angle of 9.93°, amplitude of oscillation of 4.65° at a reduced frequency of 0.064 and figure 9 presents for a mean angle of 12.25°, amplitude of 4.8°, and a reduced frequency of 0.126. The figures reproduce the corresponding ones presented in reference 35. It can be seen from these figures that (1) the lift coefficient is predicted well, (2) the maximum moment coefficient has not been obtained for the case of $k = 0.126$, and (3) moment loops are not reproduced correctly.

A close examination of the results in reference 35 for other airfoils, and for other flow conditions revealed that the prediction is good for thin airfoils at low reduced frequency and the maximum moment coefficient is not predicted.

Stall model B: Reference 38 presents synthesized lift and moment loops for 13 data sets comprising different airfoils (SC1095, NACA 0012, V0012, VR7, NLR-1, V2301-1.58, Yawed 0012), Mach numbers (0.18 to 0.6), reduced frequencies (0.0 to 0.38) and Reynold's numbers 2.5 to 6.2 million). In the present report NACA 0012 is chosen to verify the program. Figures 10 and 11 present lift and moment loops for two cases. The cases represent different mean angles, amplitude, and reduced frequency at 0.3 Mach number and Reynold's number of 3.8 million. The steady state-data for this airfoil is obtained from an analytical curve fit program available in G400PROP computer code (ref. 57). The static stall angle for Mach number 0.3 is 12°. The lift loops from this model show good correlation with experimental data over the upper portion (upstroke) but the present program under predicts the lift coefficient in the returning stroke. But the published results in reference 38 showed good comparison even in the down stroke. The reason for this discrepancy between the present theoretical results and those of reference 38 is not known at this time of writing. However, it should be noted that in a response analysis, one is interested in calculating the maximum lift obtained in dynamic stall. So the predicted loops are assumed satisfactory for this purpose. The moment loops show good correlation with the theoretical and experimental loops of reference 38. In contrast to lift loops during the down stroke, the moment loops behave well throughout the cycle. The good correlation for lift and moment loops may not be surprising since the model is actually experimental data, reconstructed by analytical curve fitted expressions, which naturally takes into account all the events that occur in a dynamic stall process.

Stall model C: The ONERA model was first fitted for the OA212 airfoil (ref. 39). This airfoil has a lift stall angle of 10° and a moment stall angle of 6°. The results are presented for a Mach number of 0.3 and reduced frequency of 0.05, with amplitude of oscillation of 6° for mean angles of attack of 12° and 14°. The governing equations are solved using a fourth order Runge-Kutta method. Figures 12 and 13 with designation "a" show the lift loops obtained from this model with and without stall delay for mean angles of 12° and 14°. The model with stall delay predicted the maximum lift coefficient well. The lift loops calculated herein are in good agreement with corresponding ones in reference 39. The moment loops for the same cases are presented in figures 12 and 13 with designation "b". Again, the results show good correlation with those published in reference 39. Introducing stall delay did not improve the correlation since the range of angle of attack studied is well above the moment stall angle of 6°. It is interesting to note that the moment curves (even the experimental ones) did not show any loops for this airfoil.

Comparison of the three dynamic stall models for a single airfoil. - In this section, the three dynamic stall models are applied for a particular airfoil. In this case, NACA 0012 airfoil, at Mach number = 0.3, and Reynold's number of 3.8 million is considered.

For NACA 0012 airfoil, the lift loops from model B are presented earlier, and they are calculated here for models A and C. In generating these plots, the static stall angle for lift is assumed as 12° for models A and B, and 14° for model C. To compare all these results, all three loops are shown in

figures 14 to 17, for four cases by varying the mean angle of attack, amplitude of oscillation, and reduced frequency. These cases are listed below.

Case 1: $\alpha_0 = 10°$ $\bar{\alpha} = 10°$, $k = 0.04813$

Case 2: $\alpha_0 = 12°$, $\bar{\alpha} = 10°$, $k = 0.09756$

Case 3: $\alpha_0 = 12°$, $\bar{\alpha} = 8°$, $k = 0.12528$

Case 4: $\alpha_0 = 15°$, $\bar{\alpha} = 5°$, $k = 0.15106$

The measured lift loops are also included in figures 14 to 17. The plots obtained from dynamic stall models A, B, and C are designated by a, b, and c, respectively. To facilitate comparison, the experimental plots are also shown in the figures.

Figure 14 shows the lift loops obtained for case 1. All three stall models predict the loops reasonably well for this reduced frequency of 0.048. Even the simplest model, model A, gives a very good correlation between theory and experiment. Model B, as mentioned in the previous section underpredicts the lift coefficient during the down stroke. The ONERA model, model C, predicts a high lift coefficient compared to models A, B, and experiment. This may be due to the assumption of high static stall angle for the airfoil, and may be due to the numerical procedure required in integrating the equations.

Figure 15 presents the plots for case 2. The reduced frequency for this case is approximately twice that for the previous case. The amplitude of oscillation is 10°, as in the previous case. It can be seen from plot 'a' that model A did not qualitatively reproduce the experimental curve, even though the maximum lift coefficient is reasonably well predicted. Since the area of the loop represents the energy transfer, or damping in the system, this model underpredicts the damping. Models B and C predict the loop reasonably well.

Figure 16 shows the lift loops obtained for case 3. The reduced frequency and the amplitude of oscillation are 0.125 and 8° respectively. Models A and C predict a larger maximum lift coefficient and model B predicts a lower maximum lift coefficient compared to experiment.

Figure 17 shows the plots for case 4. The reduced frequency is 0.151, and the amplitude of oscillation is 5°. It is surprising to note that model A predicts the lift loop reasonably well compared to experiment. Model C predicts a larger lift loop.

An overall comparison of the figures 14 to 17 indicate that all three dynamic stall models predicted the lift loops reasonably well for the cases considered. However, the following note is in order regarding the application of model C. The parameters in model C have been evaluated from tests conducted at small amplitude of oscillation ($\approx 1°$). Here the model has been used for predicting lift at high amplitude of oscillation ($\geq 5°$). This model is expected to give still better correlation with experimental data when used in a small amplitude of oscillation environment, such as that exists for propellers and compressors. Models A and B do not have such restrictions on formulation and use.

Moment Coefficient

Figures 18 to 21 show the moment loops obtained from models A and B. Specifically, in these figures, plots (a) and (b) show the loops obtained from models A and B, respectively. Since the moment data is not available for NACA 0012 from the ONERA fit, loops from this model are not shown. The plots are presented for mean angles of attack of 10°, 12°, and 15°, amplitude of oscillation of 10° and 5°, and reduced frequencies of 0.09756, 0.09633, and 0.151. An overall observation of the figures 18 to 21 shows that the moment loops are not predicted well by model A. The experimental data shows three loops. Model A predicts only two loops. Since the area of the curve is proportional to the damping in the system (or energy dissipated/absorbed), stall response curves from model A may not be accurate. For model B, there is a very good correlation between calculated and measured results. This should be expected with this model, because these loops are curve-fitted to experimental data.

Aeroelastic Response Studies with Dynamic Stall Models

The following sections present the results of the response study conducted with two structural models, a typical section model and a plate model. Both models perform plunging and pitching oscillations. For a given airfoil, the comparison of the limit cycle behavior with both pitching and plunging oscillations from the three dynamic stall models would have been ideal. However, the moment data is not available for NACA 0012 from model C, for a comparative study. Therefore response from plunging only is considered for comparison purpose of the three dynamic stall models. However, for models A and B, both plunging and pitching are considered and compared. The governing equations are solved by the Wilson-θ method (ref. 59). This method assumes a linear variation of acceleration between two time steps. The method is an implicit integration method and is unconditionally stable.

Plunging motion only. - The NACA 0012 airfoil at a Mach number of 0.3 is considered for the numerical study. The response curves are obtained for zero initial conditions with a time step equal to or less than the 1/10th of the minimum period of oscillation. The variation of the angle of attack with time is given by $\alpha = \alpha_0 + \dot{h}/V$, where h is the plunging displacement.

Typical Section Model

The governing differential equation for this case is equation (30). The values of the parameters in the equation are, mass ratio, $\mu = 76$, $\omega = 40.0$ rad/sec, and $\omega_h = 55.9$ rad/sec. Figure 22 shows the variation of plunging displacement with time at an initial angle of attack of 4.5° obtained from the three models. The response from the three models shows a converging trend towards a steady value. Figure 23 shows the variation of plunging displacement with time when the initial angle of attack is 15°. The models predict different behavior. Model A shows a small amplitude limit cycle behavior, model B shows a converged solution. This is due to the fact that model B includes unsteady aerodynamic effects, and hence predicts a higher stall flutter speed. Model C shows a high amplitude limit cycle behavior since the model in general overpredicts the lift for this airfoil as shown in the previous section.

Plate Model

Equation (44) is the governing equation of motion for this case with $i = 1$. The values of m_1, and ω_1 are 0.972×10^{-5} lb-sec^2/in. and 999.0 rad/sec. Figures 24 and 25 present the plunging response obtained from the plate model. Figure 24 shows the response obtained from the three dynamic stall models for an initial angle of attack of 4.5°. All three dynamic stall models predict a converging solution. Figure 25 shows the response obtained for an initial angle of attack of 15°. The behavior is as that predicted above for the typical section model.

Pitching and Plunging Oscillations

Typical Section Model

The governing equations for this combined bending and torsion are given by equation (32). The numerical study is conducted for the following structural parameters.

$\mu = 76.0$, $\bar{x}_\alpha = 0.25$, $a_h = -0.15$, $r_\alpha = 0.6229$,

$\omega_h = 55.9$ rad/sec, $\omega_\alpha = 64.1$ rad/sec, $\zeta_h = 0.0$,

$\zeta_\alpha = 0.0$, $b = 0.127$ m (5")

For these values, the model has both inertial coupling and aerodynamic coupling between the plunging and pitching motions. Before starting the response analysis, it was necessary to find the aeroelastic parameters corresponding to a neutrally stable condition. Hence, a classical flutter analysis was performed in the frequency domain by using two-dimensional unsteady aerodynamic theory. This predicted the flutter speed, V_F, as 27.46 m/sec (90.1 ft/sec), and reduced frequency, k_F, as 0.27624. The corresponding velocity parameter, U_F^*, is given by

$$U_F^* = \frac{V_F}{b\omega_\alpha} = 3.3735$$

and this flutter speed corresponds to a Mach number of 0.0811.

In the present time domain analysis, the response analysis was carried out by varying U^*, keeping the values of other parameters constant. The static data corresponds to a NACA 0012 airfoil, at a Mach number of 0.3 and Reynold's number of 3.8 million. The static stall angle for this airfoil is 12°. The initial conditions are taken as $\xi' = 0.$, $\xi = 0.$, $\alpha' = 0.$, and $\alpha = 0.01$ rad. A time step equal to or less than 1/10th of the minimum period of oscillation is used in the calculations.

Figure 26a shows the variation of pitching displacement with time when the airfoil is at an initial angle of 4.5°, obtained from model A. It should be noted that for this angle of attack, which is below the static stall angle, the aerodynamic theory in model A corresponds to quasi-steady theory. The plot shows three graphs that correspond to $U^* = 2.50$, 2.675 and 2.75. The graph corresponding to $U^* = 2.50$, shows converging oscillations, whereas

the one for U^* = 2.675, shows sinusoidal oscillations. This is assumed to be indicating neutral stability, since the angle of attack variation for this case is well below the static stall angle. The graph for U^* = 2.75, shows diverging oscillations. The value of U^* = 2.675 is taken as the one corresponding to the flutter speed. This is 21 percent less than the value predicted from unsteady theory, showing that quasi-steady theory underpredicts the flutter speed. Figure 26b shows the variation of plunging displacement with time. It exhibits the same behavior as the pitching displacement.

Figure 27 shows the response curves obtained from model B for the same structural parameters and for the same initial angle of attack. It should be noted that the unsteady parameters (below stall) available for NACA 0012 at a Mach number of 0.3 are used in the response calculation. Figure 27a shows two graphs that correspond to U^* = 3.17, and 3.18. The graph corresponding to U^* = 3.17, shows converging oscillations, whereas the one for U^* = 3.18, shows diverging oscillations indicating instability of the motion. Hence the value of U^* = 3.175 corresponds to flutter speed. This is 6 percent less than the value predicted from unsteady theory in the frequency domain. Figure 27b shows the variation of plunging displacement with time for the same parameters as above. It exhibits the same behavior as the pitching displacement.

Figures 28 and 29 show the response curves obtained from models A and B for an initial angle of attack of 15°. This is above the static stall angle of 12° for NACA 0012. The other parameters used in stalled airloads calculation are Re = 3.8 million and Mach number = 0.3.

Figure 28 shows the variation of pitching displacement with time when the airfoil is at an initial angle of 15°. Figure 28a is the response curve obtained from model A. The plot shows two graphs that correspond to U^* equal to 0.1 and 0.2. Both the graphs show that the transients (due to nonzero initial acceleration and nonzero initial displacement) die out in a certain amount of time and then the oscillation starts growing indicating unstable oscillations. It is seen from figure 28a that the time for the transients to die out is inversely proportional to the velocity parameter, U^*. Response curves generated with zero initial conditions (zero velocity and zero displacement), not shown here, indicated that the oscillations start to diverge immediately. This indicates that flutter begins essentially at zero speed compared to U^* = 2.75 at an initial angle of 4.5°. However, this physically unreasonable result is not surprising, since this model did not predict the moment loops correctly for this airfoil which resulted in negative damping.

Figure 28b is the response curve obtained from model B, for the same structural and aerodynamic parameters. The plot shows two graphs, one for U^* = 0.45 and the other for U^* = 0.5. The graph for U^* = 0.45 shows decaying oscillations indicating stable oscillations. The graph for U^* = 0.5 shows that the airfoil is set into a limit cycle behavior. The decay of the transient and the motion being set into a limit cycle is more clearly seen here, compared to that shown in figure 28a obtained from model A. The critical stall flutter speed corresponds to U^* = 0.475, the average of the above two values. This is 85 percent reduction in flutter speed compared to 3.175 at an initial angle of 4.5°.

Figure 29 shows the variation of plunging displacement with time, and it shows the same variation with time as pitching motion for both the models.

Plate Model

The response of the plate is analyzed using normal modes. These normal modes are obtained from a NASTRAN analysis. The plate is 3 in. in length, 1 in. in width (chord) and 0.05 in. thick. The material density is 2.6×10^{-4} lb sec^2/in^4, Young's modulus 7.89×10^6 lb/in^2 and Poisson's ratio 0.3. The analysis used QUAD4 elements. In the present study, two normal modes are used in the analysis. For this problem, the first and second normal modes are essentially the first bending and the first torsion modes. From the NASTRAN analysis, the first two generalized masses are 0.9720×10^{-5} lb sec^2/in. and 0.161×10^{-5} lb sec^2/in., and the corresponding frequencies are 999.2 rad/sec and 5860.55 rad/sec. The NACA 0012 airfoil at Mach number 0.3 is considered for the aeroelastic study. The governing equations of motion are given by equation 44. The response is calculated with the following initial conditions: $q_1 = q_1' = q_2' = 0.0$ and $q_2 = 0.01$, where q_1 and q_2 represent the first two normal coordinates and q_1' and q_2' their derivative with nondimensional time. The variation of the normal coordinates with time is shown in figures 30 to 33.

Figure 30 shows the variation of the first normal coordinate (the first bending mode) with time when the flow is approaching the plate at an initial angle of attack of 4.5°. Since the initial angle of attack is below static stall angle (12° for this airfoil), the response is a quasi-steady response for model A. Both models predict the same qualitative behavior, even though model B predicts a slightly lower amplitude due to unsteady effects included in the model. The response is seen to decay indicating an approach to steady displacement. Figure 31 shows the variation of the second normal coordinate (first torsion) with time at the same initial angle of attack. The response again seen converging to a steady value.

Figures 32 and 33 show the variation of first and second normal coordinates, respectively, with time when the initial angle of attack is 15°, which is above the static stall angle. Both models predict a diverging type of oscillation. This means that the plate is unstable for this initial angle of attack. Further investigation is required to predict the stall flutter boundary from both models with other initial angles of attack varying from 4.5° to 15°. However, it can be noted from previous sections that model B predicts a higher initial angle of attack than model A for the plate to become unstable.

DISCUSSION OF ADVANCED TURBOPROP APPLICATION

The theory and the computer program presented in this report can be directly applied to predict the response of an advanced turboprop with dynamic stall. However, proper blade data for the advanced turboprop airfoil is needed. Figure 34 shows the airfoil section distribution for SR2 advanced turboprop. The thickness ratio (t/b), twist ($\Delta\beta$), design lift coefficient (C_{LD}), and planform (b/D) distribution were established to provide for high efficiency. The airfoil sections used are NACA 16 series from tip to the 45 percent radius portion, and 65 series with circular arc (CA) camber lines

from 37 percent radius to the root with a transition fairing in between. These airfoils have been chosen for their high critical Mach number and wide, low drag buckets. This necessitates generation of static and dynamic data for a number of airfoils along the radius.

The operating conditions of the advanced turboprop indicate that the advanced turboprop blades are subject to high frequency, low amplitude oscillations. This is a favorable condition for light dynamic stall, since the penetration of the airfoil into stall is small, and the duration in the stall condition is small, even when it is operating at static stall angles. This does not allow the boundary layer to reach the leading edge or the formation of a vortex like disturbance. This implies that models A and C may predict the stall behavior of advanced turboprop reasonably well. Also as mentioned in earlier sections, model C has been formulated under the assumption of small amplitude. From the theoretical analysis point of view, boundary-layer methods, rather than full Navier-Stokes solutions may be sufficient for advanced turboprop application. However, it should be cautioned that light dynamic stall is very sensitive, to airfoil shape, particularly, and to the leading edge radius. Depending on this radius, the flow may separate at the leading edge and may result in deep stall. It is worthwhile here to mention the conclusions drawn from an experimental study of stall flutter characteristics of NACA 16 series in reference 60. The study indicated that: (1) an increase in camber, thickness ratio or design lift coefficient increases the static stall angle, (2) an increase in leading edge radius or in the droop has a slightly detrimental effect on stall, and (3) an addition of trailing edge camber increases normal force coefficient before stall.

An extensive literature search has found that no static data at and beyond stall and no dynamic data exists for 16 series airfoil. Hence the following procedure is recommended to obtain static and the dynamic data to use for advanced turboprop analysis. Generate the steady data and a single dynamic loop data for a representative NACA 16 series airfoil using Navier-Stokes solution methods (ref. 17). Then develop the ONERA dynamic stall model from the data obtained from the Navier Stokes code. Use this ONERA Navier-Stokes model to calculate the stall induced loads at all sections along the radius when the angle of attack exceeds the static stall angle. Then compare the response of the advanced turboprop obtained from the ONERA Navier-Stokes dynamic stall model, and model A.

SUMMARY AND CONCLUSIONS

Three dynamic stall models are compared for performance and easy implementation. The response of a typical section model and a plate model are studied for these stall models. The procedure and the computer program can be directly used to analyze the response of advanced turboprops with dynamic stall.

In summary:

1. All three dynamic stall models are implemented in a computer program and the program is checked out.

2. All three dynamic stall models are applied to a single airfoil to calculate lift and where possible moment loops, and the strong and weak points of these models in predicting the stall behavior are identified and discussed.

3. Stall flutter response is calculated by using all three dynamic stall models and two structural models.

4. A formulation for the stall flutter analysis code for advanced turboprop is suggested.

The following conclusions are drawn from this study:

1. The operating environment of an advanced turboprop favors the condition of light stall, where the vortex induced loads are not very severe. Therefore, simple dynamic stall models like model A and model C can be used for advanced turboprop application.

2. The ONERA model, model C, involves fewer parameters in modeling the dynamic stall model than the synthesis procedure, model B. Model A involves only one empirical parameter but must be tested for advanced turboprop airfoils and high-frequency low amplitude oscillations that occur in advanced turboprops.

3. The differential form of the ONERA model suggests that it could be used in a linearized stability analysis.

APPENDIX A

AEROELASTIC EQUATIONS WITH ONERA DYNAMIC STALL MODEL (MODEL C)

This appendix presents the state vector form of the combined structural-stall model for a typical section model and a plate model with ONERA dynamic stall model (model C).

A.1 Typical Section Model

The governing equations of the typical section are given by equation (32), and can be written as (with multiplication factors absorbed into the matrices)[+]

$$[M]\begin{Bmatrix}\xi\\ \alpha_p\end{Bmatrix}'' + [C]\begin{Bmatrix}\xi\\ \alpha_p\end{Bmatrix}' + [K]\begin{Bmatrix}\xi\\ \alpha_p\end{Bmatrix} = \begin{bmatrix}\cos\alpha & 0.0\\ (a_h + 0.5)\cos\alpha & 2.0\end{bmatrix}\begin{Bmatrix}c_\ell\\ c_{mc/4}\end{Bmatrix} \qquad (A.1.1)$$

where α is the angle of attack, and operator $()'$ indicates derivative with respect to $\bar{t}$ $(= \omega t)$.

From ONERA formulation, c_ℓ and $c_{mc/4}$ are given by equations (20c) and (20f) as

$$\begin{Bmatrix}c_\ell\\ c_{mc/4}\end{Bmatrix} = \begin{Bmatrix}0\\ C_{M1}\end{Bmatrix} + \begin{bmatrix}1.0 & 1.0 & 0.0 & 0.0 & 0.0\\ 0.0 & 0.0 & 0.0 & 1.0 & 0.0\end{bmatrix}\begin{Bmatrix}C_{L1}\\ C_{l2}\\ C'_{l2}\\ C_{M2}\\ C'_{M2}\end{Bmatrix} \qquad (A.1.2)$$

Substituting equation (A.1.2) in equation (A.1.1), we obtain

[+]Note 1: α_p is the pitching degree of freedom, subscript p is used to distinguish it from α, the instantaneous angle of attack.
Note 2: The transformation from the operator $()^*$ to $()'$ is $()^* = k()'$, where $k = \frac{\omega b}{V}$, ω = reference frequency, b is semi-chord and V is reference velocity.
Note 3: The multiplication factors include $0.5\,\rho V^2 c$ and $0.5\,\rho V^2 c^2$ to get actual lift and moment.

$$[M]\begin{Bmatrix}\xi\\ \alpha_p\end{Bmatrix}'' + [C]\begin{Bmatrix}\xi\\ \alpha_p\end{Bmatrix}' + [K]\begin{Bmatrix}\xi\\ \alpha_p\end{Bmatrix} = \begin{bmatrix}-\cos\alpha & 0.0\\ (a_h + 0.5)\cos\alpha & 2.0\end{bmatrix}$$

$$\left[\begin{Bmatrix}0\\ C_{M1}\end{Bmatrix} + \begin{bmatrix}1.0 & 1.0 & 0.0 & 0.0 & 0.0\\ 0.0 & 0.0 & 0.0 & 1.0 & 0.0\end{bmatrix}\begin{Bmatrix}C_{L1}\\ C_{L2}\\ C'_{L2}\\ C_{M2}\\ C'_{M2}\end{Bmatrix}\right] \qquad (A.1.3)$$

Let

$$A_5 = \begin{bmatrix}-\cos\alpha & 0.0\\ (a_h + 0.5)\cos\alpha & 2.0\end{bmatrix} \text{ and } B_5 = \begin{bmatrix}1.0 & 1.0 & 0.0 & 0.0 & 0.0\\ 0.0 & 0.0 & 0.0 & 1.0 & 0.0\end{bmatrix}$$

$$[M]\begin{Bmatrix}\xi\\ \alpha_p\end{Bmatrix}'' + [C]\begin{Bmatrix}\xi\\ \alpha_p\end{Bmatrix}' + [K]\begin{Bmatrix}\xi\\ \alpha_p\end{Bmatrix} = [A_5]\left[\begin{Bmatrix}0\\ C_{M1}\end{Bmatrix} + [B_5]\begin{Bmatrix}C_{L1}\\ C_{L2}\\ C'_{L2}\\ C_{M2}\\ C'_{M2}\end{Bmatrix}\right] \qquad (A.1.4)$$

where C_{L1}, C_{L2}, C'_{L2}, C_{M1}, C_{M2}, C'_{M2} are given by equations (20a) to (20f) as

$$C'_{L1} + \frac{\lambda_L}{k} C_{L1} = \frac{\lambda_L C_{L\ell}}{k} + \lambda_L s_L \theta' + \sigma_L \alpha' + s_L k\theta''$$

$$C''_{L2} + \frac{a_L}{k} C'_{L2} + \frac{r_L}{k^2} C_{L2} = -\left(k^2 r_L \Delta C_L + \frac{E_L}{k}\alpha'\right)$$

$$C_{M1} = C_{M\ell} + s_M k\theta' + \sigma_M \alpha' k + s_M k^2 \theta''$$

$$C''_{M2} + \frac{a_M}{k} C'_{M2} + \frac{r_M}{k^2} C_{M2} = -\left(k^2 r_M \, \Delta C_M + \frac{E_M}{k} \alpha' \right) \qquad (A.1.5)$$

where subscripts L and M are used to indicate lift and moment coefficients.

Combining equations (A.1.4) and (A.1.5) and writing it in state vector form, we obtain

$$\begin{Bmatrix} \xi' \\ \alpha_p' \\ \xi'' \\ \alpha'' \\ C'_{L1} \\ C'_{L2} \\ C''_{L2} \\ C'_{M2} \\ C''_{M2} \end{Bmatrix} = \begin{bmatrix} [0] & [I] & [0] & \\ -[M]^{-1}[K] & -[M]^{-1}[C] & [M]^{-1}[A_5][B_5] & \\ & & \frac{-\lambda_L}{k} \quad 0.0 \quad 0.0 & \\ [0] & & 0.0 \quad 0.0 \quad 1.0 & [0] \\ & & 0.0 \quad \frac{-r_L}{k^2} \quad \frac{-a_L}{k} & \\ & & & 0.0 \quad 1.0 \\ [0] & & [0] & \\ & & & \frac{-r_M}{k^2} \quad \frac{-a_M}{k} \end{bmatrix} \begin{Bmatrix} \xi \\ \alpha_p \\ \xi' \\ \alpha' \\ C_{L1} \\ C_{L2} \\ C'_{L2} \\ C_{M2} \\ C'_{M2} \end{Bmatrix} + \begin{Bmatrix} [0] \\ [M]^{-1}[A_5] \begin{Bmatrix} 0 \\ C_{M1} \end{Bmatrix} \\ \frac{\lambda_L C_{L\ell}}{k} + \lambda_L s_L \theta' + \sigma_L \alpha' + s_L k \theta'' \\ 0.0 \\ -\left(k^2 r_L \, \Delta C_L + \frac{E_L}{k} \alpha' \right) \\ 0.0 \\ -\left(k^2 r_M \, \Delta C_M + \frac{E_M}{k} \alpha' \right) \end{Bmatrix} \qquad (A.1.6)$$

Defining

$$Y = \left\{ \xi, \ \alpha_p, \ \xi', \ \alpha_p', \ C_{L1}, \ C_{L2}, \ C'_{L2}, \ C_{M2}, \ C'_{M2} \right\},$$

equation (A.1.6) can be written as

$$\{Y\}' = [A]\{Y\} + \{G\} \qquad (A.1.7)$$

A.2 Plate Model (Continuum Model)

The governing equations of motion, formulated in terms of normal coordinates, are given by equation 44 as

$$m_i \ddot{q}_i + m_i \omega_i^2 q_i = Q_i \qquad i = 1,2, \ldots NM \tag{A.2.1}$$

where m_i, ω_i, q_i, Q_i are respectively the generalized mass, circular frequency, normal coordinate, generalized force in i^{th} normal mode, and NM is the number of normal modes used in the analysis.

The generalized force, Q_i, is given by the following equation

$$Q_i = \int_0^{\ell} L(y,t)\, h_i(y)dy + \int_0^{\ell} M(y,t)\, \alpha_i\,(y)dy \tag{A.2.2}$$

where $L(y,t)$ and $M(y,t)$ are the normal force and pitching moment at y at time t, ℓ is the length of the plate, h_i and α_i are the normal modes in plunging and pitching in i^{th} mode.

Let the plate be divided into N number of segments. Then Q_i can be evaluated as

$$Q_i = \sum_{j=1}^{N} \left[h_i(y_j)dy_j L_j(y_j,t) + \alpha_i(y_j)dy_j M_j(y_j,t) \right] \tag{A.2.3}$$

where j indicates the j^{th} segment, dy_j is the length of the j^{th} segment, $h_i(y_j)$ and $\alpha_i(y_i)$ are the normal modal values at station y_j. Equation (A.2.1) for NM normal modes can be written as

$$[M]\{\ddot{q}\} + [K]\{q\} = \{Q\}$$

where

$$[M] = \lceil m_1, m_2, \ldots m_i, \ldots m_{NM} \rfloor, \qquad [K] = \lceil m_1\omega_1^2, m_2\omega_2^2, \ldots m_i\omega_i^2, \ldots m_{MN}\omega_{NM}^2 \rfloor$$

$$\{q\} = (q_1, q_2, \ldots q_i, \ldots q_{NM}) \quad \text{and} \quad \{Q\} = (Q_1, Q_2, \ldots Q_i, \ldots Q_{NM})$$

The vector {Q} is given by

$$
\begin{Bmatrix} Q_1 \\ Q_2 \\ \vdots \\ Q_i \\ \vdots \\ Q_{NM} \end{Bmatrix} = \begin{bmatrix} h_1(y_1)dy_1 & \alpha_1(y_1)dy_1 & h_1(y_2)dy_2 & \alpha_1(y_2)dy_2 & \cdots & h_1(y_N)dy_N & \alpha_1(y_N)dy_N \\ h_2(y_1)dy_1 & \alpha_2(y_1)dy_1 & h_2(y_2)dy_2 & \alpha_2(y_2)dy_2 & \cdots & h_2(y_N)dy_N & \alpha_2(y_N)dy_N \\ \vdots & \vdots & \vdots & \vdots & & \vdots & \vdots \\ h_i(y_1)dy_1 & \alpha_i(y_1)dy_1 & h_1(y_2)dy_2 & \alpha_1(y_2)dy_2 & \cdots & h_1(y_N)dy_N & \alpha_i(y_N)dy_N \\ \vdots & \vdots & \vdots & \vdots & & \vdots & \vdots \\ h_{NM}(y_1)dy_1 & \alpha_{NM}(y_1)dy_1 & h_{NM}(y_2)dy_2 & \alpha_{NM}(y_2)dy_2 & \cdots & h_{NM}(y_N)dy_N & \alpha_{NM}(y_N)dy_N \end{bmatrix}
$$

(Number of normal modes ↓; Number of segments →)

NM * 2N

$$
\times \begin{Bmatrix} L_1(y_1,t) \\ M_1(y_1,t) \\ L_2(y_2,t) \\ M_2(y_2,t) \\ \vdots \\ L_j(y_j,t) \\ M_j(y_j,t) \\ \vdots \\ L_N(y_N,t) \\ M_N(y_N,t) \end{Bmatrix} \qquad (A.2.4.1)
$$

2N * 1

or

$$\{Q\} = [B_6]\{F\} \qquad (A.2.4.2)$$

The lift and moment at each segment are related to their coefficients as

$$\begin{Bmatrix} L_1 \\ M_1 \\ L_2 \\ M_2 \\ \vdots \\ L_j \\ M_j \\ \vdots \\ L_N \\ M_N \end{Bmatrix} = \begin{Bmatrix} [A_5] \begin{Bmatrix} 0 \\ C_{M1} \end{Bmatrix}_1 \\ [A_5] \begin{Bmatrix} 0 \\ C_{M1} \end{Bmatrix}_2 \\ \vdots \\ [A_5] \begin{Bmatrix} 0 \\ C_{M1} \end{Bmatrix}_j \\ \vdots \\ [A_5] \begin{Bmatrix} 0 \\ C_{M1} \end{Bmatrix}_N \end{Bmatrix} + \begin{bmatrix} [A_5]_1 & 0 & 0 & 0 \\ 0 & [A_5]_2 & 0 & 0 \\ \vdots & \vdots & \vdots & \vdots \\ 0 & 0 & [A_5]_j & 0 \\ \vdots & \vdots & \vdots & \vdots \\ 0 & 0 & 0 & [A_5]_N \end{bmatrix} \begin{Bmatrix} c_{\ell 1} \\ c_{m1} \\ c_{\ell 2} \\ c_{m2} \\ \vdots \\ c_{\ell j} \\ c_{mj} \\ \vdots \\ c_{\ell N} \\ c_{mN} \end{Bmatrix} \qquad \text{(A.2.5)}$$

or

$$\{F\} = \{A_{cp}\} + [A_{5p}]\{X\}$$

The coefficients $c_{\ell 1}$, c_{m1}, ... $c_{\ell j}$, c_{mj} of each segment are given by

$$\begin{Bmatrix} c_{\ell 1} \\ c_{m1} \\ c_{\ell 2} \\ c_{m2} \\ \vdots \\ c_{\ell j} \\ c_{mj} \\ \vdots \\ c_{\ell N} \\ c_{mN} \end{Bmatrix} = \begin{bmatrix} [B_5]_1 & & & & \\ & [B_5]_2 & & & \\ & & \ddots & & \\ & & & [B_5]_j & \\ & & & & [B_5]_N \end{bmatrix} \begin{Bmatrix} Z_1 \\ Z_2 \\ \vdots \\ Z_j \\ \vdots \\ Z_N \end{Bmatrix} \qquad \text{(A.2.6)}$$

or

$$\{X\} = [B_{5P}]\{Z\}$$

where $Z = \{Z_1, Z_2, \ldots Z_j, \ldots Z_N\}$ and $\{Z_j\} = \left\{c_{L1}, c_{L2}, c'_{L2}, c_{M2}, c'_{M2}\right\}_j$.

Here A_{5_j} and B_{5_j} are the A_5 and B_5 matrices of j^{th} segment defined earlier in Section A.1. The vector Z_j is given by equation A.1.5 for each segment. Substituting from equations A.1.5, A.2.6, A.2.5, A.2.4 into equation A.2.1, and writing in state vector form, the final equations are given by A.2.7, given below.

$$
\begin{Bmatrix} q' \\ q'' \\ \begin{pmatrix} C'_{L1} \\ C'_{L2} \\ C''_{L2} \\ C'_{M2} \\ C''_{M2} \end{pmatrix}_1 \\ \begin{pmatrix} C'_{L1} \\ C'_{L2} \\ C''_{L2} \\ C'_{M2} \\ C''_{M2} \end{pmatrix}_2 \\ \vdots \\ \begin{pmatrix} C'_{L1} \\ C'_{L2} \\ C''_{L2} \\ C'_{M2} \\ C''_{M2} \end{pmatrix}_N \end{Bmatrix}
=
\begin{bmatrix}
[0] \quad [I] & [0] & & \\
-[M]^{-1}[K] \quad [0] & [M]^{-1}[B_6][A_{5p}][B_{5p}] & & \\
[0] & \begin{matrix} -\frac{\lambda_L}{k_1} & 0 & 0 & 0 & 0 \\ 0 & 0 & 1.0 & 0 & 0 \\ 0 & -\frac{r_L}{k_1^2} & -\frac{a_L}{k_1^2} & 0 & 0 \\ 0 & 0 & 0 & 0 & 1.0 \\ 0 & 0 & 0 & -\frac{r_M}{k_1^2} & -\frac{a_M}{k_1^2} \end{matrix} & [0] & [0] \\
[0] & [0] & \begin{matrix} -\frac{\lambda_L}{k_2} & 0 & 0 & 0 & 0 \\ 0 & 0 & 1.0 & 0 & 0 \\ 0 & \frac{r_L}{k_2^2} & \frac{a_L}{k_2^2} & 0 & 0 \\ 0 & 0 & 0 & 0 & 0 \\ 0 & 0 & 0 & -\frac{r_M}{k_2^2} & -\frac{a_M}{k_2^2} \end{matrix} & [0] \\
[0] & [0] & [0] & \begin{matrix} -\frac{\lambda_L}{k_N} & 0 & 0 & 0 & 0 \\ 0 & 0 & 1.0 & 0 & 0 \\ 0 & -\frac{r_L}{k_N^2} & -\frac{a_L}{k_N^2} & 0 & 0 \\ 0 & 0 & 0 & 0 & 1.0 \\ 0 & 0 & 0 & -\frac{r_M}{k_N^2} & -\frac{a_M}{k_N^2} \end{matrix}
\end{bmatrix}
\begin{Bmatrix} q \\ q' \\ \begin{pmatrix} C_{L1} \\ C_{L2} \\ C'_{L2} \\ C_{M2} \\ C'_{M2} \end{pmatrix}_1 \\ \begin{pmatrix} C_{L1} \\ C_{L2} \\ C'_{L2} \\ C_{M2} \\ C'_{M2} \end{pmatrix}_2 \\ \vdots \\ \begin{pmatrix} C_{L1} \\ C_{L2} \\ C'_{L2} \\ C_{M2} \\ C'_{M2} \end{pmatrix}_N \end{Bmatrix}
+
\begin{Bmatrix} 0 \\ [M]^{-1}[B_6]\{A_{cp}\} \\ -\frac{\lambda_L}{k_1} C_{L\ell} + (\lambda_L s_L + \sigma_L)\alpha' + s_L k_1 \alpha'' \\ 0.0 \\ -\left(k_1^2 \, r_L \, \Delta C_L + \frac{E_L}{k_1} \alpha' \right) \\ 0.0 \\ -\left(k_1^2 \, r_M \, \Delta C_M + \frac{E_M}{k_1} \alpha' \right) \\ -\frac{\lambda_L}{k_2} C_{L\ell} + (\lambda_L s_L + \sigma_L)\alpha' + s_L k_2 \alpha'' \\ 0.0 \\ -\left(k_2^2 \, r_L \, \Delta C_L + \frac{E_L}{k_2} \alpha' \right) \\ 0.0 \\ -\left(k_2^2 \, r_M \, \Delta C_M + \frac{E_M}{k_2} \alpha' \right) \\ \vdots \\ -\frac{\lambda_L}{k_N} C_{L\ell} + (\lambda_L s_L + \sigma_L)\alpha' + s_L k_N \alpha' \\ 0.0 \\ -\left(k_N^2 \, r_L \, \Delta C_L + \frac{E_L}{k_N} \alpha' \right) \\ 0.0 \\ -\left(k_N^2 \, r_M \, \Delta C_M + \frac{E_M}{k_N} \alpha' \right) \end{Bmatrix}
\tag{A.2.7}
$$

where k_1, k_2, ... k_j, ... k_N are the values of the reduced frequency for each segment. The size of the matrix is (2 x NM + 5N).

APPENDIX B

DYNAMIC STALL DATA FOR MODEL B AND MODEL C

This appendix presents the dynamic stall data for model B and model C that is used in generating the hysteresis loops for the NACA 0012 airfoil. The Mach number is 0.3 and the Reynold's number is 3.8×10^6.

Model B: The following data corresponds to data set number 2 in reference 38 generated through synthesization method. The values of the parameters appearing in equations 16 to 19 are given below:

$\alpha_{ss} = 12°$

$P_1/\text{rad} = 17.988, \quad P_2/\text{rad} = 2.410, \quad P_3 = -0.1661$

$Q_1/\text{rad} = 1.8347, \quad Q_2/\text{rad} = 0.2123, \quad Q_3 = -0.0307, \quad Q_4 = -0.0966,$
$Q_5 = 0.7754, \quad Q_6/\text{rad} = 2.842, \quad Q_7/\text{rad/rad} = 7.557$

$n_1/\text{rad} = -1.782, \quad n_2/\text{rad} = -0.191, \quad n_3 = -0.0035, \quad n_4/\text{rad} = -0.0082,$

$n_5 = 0.3462, \quad n_6/\text{rad} = -1.405, \quad n_7/\text{rad/rad} = -6.354$

$\varepsilon = 0.125, \quad \bar{C}_{Am} = 3.64, \quad \bar{C}_{wm} = -0.05, \quad C_{At} = 0.084, \quad C_{\alpha t} = 0.0073,$
$\bar{C}_{AR} = 1.790, \quad \bar{C}_{wR} = -0.743.$

where $\overline{(\quad)} = (\quad)_{\alpha_{ss}}$.

Model C: Reference 58 generated the lift hysteresis loop for NACA 0012 airfoil using a single experimental loop. The values of the parameters appearing in equation 20 are given as

$\lambda = 0.2, \quad s = 0.09, \quad \sigma = 0.080 - 0.13\Delta C_L$

$C_{L\ell} = -0.01 + 0.114\,\alpha$

$C_{LS} = C_{L\ell}, \quad \alpha \leq 10°$

$C_{LS} = -0.01 + 0.114\,\alpha - 0.013\,(\alpha - 10.)^2 \quad 10° \leq \alpha \leq 14°$

$C_{LS} = 1.378 + 0.478\,(e^{-1.5(\alpha-14)} - 1) \quad \alpha > 14°$

$\sqrt{r} = 0.20 + 0.10\Delta C_L^2$

$a = 0.25 + 0.10\Delta C_L^2$

$E = -0.07\Delta C_L^2, \quad \Delta C_L = C_{L\ell} - C_{LS}$

τ_d (stall delay) $= 10, \quad (\Delta C_L = 0.208 + 0.0104\,(\alpha - 14))$

APPENDIX C

AIRFOIL STATIC DATA

In this report three airfoils, namely OA212, NACA 0012, NACA 0012(MOD), are used for the aeroelastic response study with dynamic stall. For completeness, the static data of these airfoils are presented below. The data for OA212 is presented in polynomial form, and for NACA 0012 and NACA 0012(MOD), the data is given in tabular form.

OA212 airfoil: Mach number = 0.3

Lift coefficient

$\alpha_{ss} = 10°$

$C_{L\ell} = 7.1 \frac{\pi}{180} \alpha$

$C_{LS} = 7.1 \frac{\pi}{180} \alpha \qquad (-\alpha_{ss} < \alpha < \alpha_{ss})$

$C_{LS} = \sum_{i=1}^{7} a_i (|\alpha| - 10°)^i \qquad (\alpha_{ss} < \alpha < 26)$

$= - \sum_{i=1}^{7} a_i (|\alpha| - 10°)^i \qquad (-26 < \alpha < -\alpha_{ss})$

$a_0 = 1.24, \quad a_1 = 0.124, \quad a_2 = -0.0630597, \quad a_3 = 0.01395201,$
$a_4 = -0.0017390851, \quad a_5 = 0.0001245913, \quad a_6 = -4.6842925 \times 10^{-6},$
$a_7 = 7.087973 \times 10^{-8}$

For angles greater than 26° (or < -26°), this polynomial diverges. Therefore, beyond, $|\alpha| > 26°$, a constant value of 1.26 is used.

$\Delta C_L = 0.$ for $(-\alpha_{ss} < \alpha < \alpha_{ss})$
$= C_{L\ell} - C_{LS} \quad (|\alpha| > \alpha_{ss})$

Moment coefficient

$\alpha SS = 6°$
$C_{M\ell} = \xi + p\alpha$
$C_{MS} = C_{M\ell} + \Delta C_M$

where $\xi = -0.006$, $p = -0.0014$. The difference in the linear extension and true static moment, ΔC_M, is given below:

Let $\theta_1 = 6°$, $\theta_2 = 13°$, $\theta_3 = 14.6°$, $\theta_4 = 20°$, Max = 0.0155 and Min = -0.056. Then for angle of attack, α,

between $-\theta_1$ and θ_1 $\qquad \Delta C_M = 0.$

between θ_1 and θ_2 $\qquad \Delta C_M = -\text{Max} \frac{(\alpha - \theta_1)^2}{(\theta_2 - \theta_1)^2}$

between θ_2 and θ_3 $\quad \Delta C_M = -Max - \theta(\alpha-\theta_2) + \left[3Max + (2r+q-p)(\theta_3-\theta_2)\right]*$

$$\frac{(\alpha - \theta_2)^2}{(\theta_3 - \theta_2)^2} - \left[2Max + (r + q - p)(\theta_3 - \theta_2)\right]\left[\frac{(\alpha - \theta_2)^3}{(\theta_3 - \theta_2)^3}\right]$$

between θ_3 and θ_4 $\quad \Delta C_M = -(q - p)(\alpha - \theta_3)$

$> \theta_4$ $\quad \Delta C_M = -Min + \dfrac{0.01(\alpha - \theta_4)}{\alpha - \theta_4 - \dfrac{0.01}{q - p}}$

where $r = \dfrac{2Max}{\theta_2 - \theta}$ $\quad q = \dfrac{Min + p(\theta_4 - \theta_3)}{\theta_4 - \theta_3}$

NACA 0012(MOD) airfoil: The data is presented for two Mach numbers. The c_ℓ and $c_{mc/4}$ with α are given in α, c_ℓ (or $c_{mc/4}$) pairs. α_{ss} is static stall angle, $a_{o\ell}$ is lift curve slope, and a_{om} is moment curve slope. α is in degrees, c_ℓ and $c_{mc/4}$ are per degree.

The following static data is for a Mach number of 0.4.

$\alpha_{ss} = 9°$, $a_{o\ell} = 6.6463$/rad, $a_{om} = 0.$

Data c_ℓ/(0.0, 0.0), (1.74, .196), (3.65, .414), (5.55, .657), (7.56, .891), (9.48, 1.081), (11.37, .957), (13.35, .853), (15.15, .812), (19.08, .951), (23.94, 1.057)

Data $c_{mc/4}$/(0., 0.), (1.74, -.018), (3.65, -.013), (5.55, -.016), (7.56, -.001), (9.48, -0.002), (11.37, -.096), (13.35, -.126), (15.15, -.127), (19.08, -.152), (23.94, -.182)

The following static data is for a Mach number of 0.6.

$\alpha_{ss} = 5.6°$, $a_{o\ell} = 8.48$/rad, $a_{om} = 0.$

Data c_ℓ/(0.0, 0.0), (1.65, .256), (3.54, .536), (4.51, .679), (5.6, .768), (7.44, .889), (9.34, .921), (11.26, .939), (14.96, 1.071), (18.12, 1.025), (18.86, 1.042)

Data $c_{mc/4}$/(0.0, 0.), (1.65, 0.), (3.54, -.001), (4.51, .006), (5.6, .008), (7.44, -.013), (9.34, -.053), (11.26, -.058), (14.96, -.123), (18.12, -.127), (18.86, -.134), (40., -.134)

NACA 0012 airfoil: The data is presented for two Mach numbers. The c_ℓ and $c_{mc/4}$ with α are given in α, c_ℓ (or $c_{mc/4}$) pairs. α_{ss} is static stall angle, $a_{o\ell}$ is lift curve slope, and a_{om} is moment curve slope. α is in degrees, c_ℓ and $c_{mc/4}$ are per degree.

The following static data is for a Mach number of 0.3.

$\alpha_{ss} = 12°$, $a_{o\ell} = 6.30254$/rad, $a_{om} = 0.$

Data c_{ℓ}/(0., 0.), (.5, .05695), (1., .1139), (2.0, .227), (4., .452), (5., .563), (6., .672), (8., .883), (9., .983), (10., 1.079), (11., 1.168), (11.5, 1.209), (12., 1.246), (12.5, 1.2757), (13., 1.293), (13.5, 1.28), (14., 1.229), (14.5, 1.1376), (15., 1.066), (15.5, 1.0343), (16., 1.0097), (17., .9255), (19., .9369), (21., .948)

Data $c_{mc/4}$/(0., 0.), (1., .00002), (2.0, .00004), (4., .000051), (5., .000032), (6., .0), (6.5, -.000014), (7., -.000031), (8., -.000057), (9., -.000047), (9.5, -.000015), (10, .00004), (10.5, .00012), (11., .000284), (12., .000164), (12.5, -.0005565), (13., -.002985), (13.5, -.00974), (14., -.02495), (15., -.0665), (16., -.07819), (18., -.08931), (20.0, -.09839), (22., -.10855)

The following static data is for a Mach number 0.4.

α_{ss} = 9°, $a_{0\ell}$ = 8.944/rad, a_{0m} = 0.0015

Data c_{ℓ}/0., 0.), (.5, .05928), (1., .1185), (2.0, .23652), (4., .46905), (5., .58237), (6., .6927), (8., .89991), (9., .99295), (10., 1.0737), (11., 1.1321), (11.5, 1.1464), (12., 1.1459), (12.5, 1.1296), (13., 1.106), (13.5, 1.09), (14., 1.0865), (14.5, 1.0851), (15., 1.0736), (15.5, 1.0433), (16., 1.0121), (17., 1.0112), (19., 1.0095), (21., 1.0078), (25., 1.0043)

Data $c_{mc/4}$/0., 0.), (1., -.00012944), (2.0, -.00025587), (4., -.00047534), (5., -.0005414), (6., -.00054157), (6.5, -.00050136), (7., -.0004223), (8., -.0000978), (9., .00054897), (9.5, .00102), (10., .0015638), (10.5, .0020693), (11., .0022224), (12., -.00232), (12.5, -.010679), (13., -.024558), (13.5, -.04069), (14., -.05433), (15., -.071335), (16., -.0828), (18., -.090655), (20.0, -.099564), (22., -.10953), (25., -.12647)

REFERENCES

1. Baker, J.E.: The Effects of Various Parameters, Including Mach Number, on Propeller Blade Flutter with Emphasis on Stall Flutter, NACA TN-3357, 1955.

2. Kaza, K.R.V.; and Kielb, R.E.: Flutter of Turbofan Rotors with Mistuned Blades, AIAA J., vol. 22, no. 11, Nov. 1984, pp. 1618-1625.

3. Mehmed, O., et al: Bending-Torsion Flutter of a Highly Swept Advanced Turboprop, NASA TM-82975, 1982.

4. Mehmed, O.; and Kaza, K.R.V.: Experimental Classical Flutter Results of a Composite Advanced Turboprop Model. NASA TM-88792, 1986.

5. Jones, B.M.: Stalling. J.R. Aeronaut. Soc., vol. 38, no. 285, Sept. 1934, pp. 753-770.

6. McCullough, G.B.; and Gault, D.E.: Examples of Three Representative Types of Airfoil-Section Stall at Low Speed. NACA TN-2502, 1951.

7. Carr, L.W.; McAlister, K.W.; and McCroskey, W.J.: Analysis of the Development of Dynamic Stall Based on Oscillating Airfoil Experiments. NASA TN D-8382, Jan. 1977. (Also, McCroskey, W.J.; Carr, L.W.; and McAlister, K.W.: Dynamic Stall Experiments on Oscillating Airfoils. AIAA J., vol. 14, no. 1, Jan. 1976, pp. 57-63.)

8. Halfman, R.L.; Johnson, H.C.; and Haley, S.M.: Evaluation of High-Angle-of-Attack Aerodynamic-Derivative Data and Stall-Flutter Prediction Techniques. NACA TN 2533, 1951.

9. Sisto, F.: Stall-Flutter in Cascades. J. Aeronaut. Sci., vol. 20, no. 9, Sept. 1953, pp. 598-604. (Also, Sisto, F.: Stall Flutter, A Modern Course in Aeroelasticity, E.H. Dowell, ed., Chapter 5, Sijthoff and Noordhoff, Rijn, The Netherlands, 1980.)

10. Schniltger, J.R.: Single Degree of Freedom Flutter of Compressor Blades in Separated Flow. J. Aeronaut. Sci., vol. 21, no.1, Jan. 1954, pp. 27-36.

11. Amer, K.B.; and LaForge, S.: Effects of Blade Stall on Helicopter Rotor Blade Bending Loads. American Helicopter Society 21st Annual National Forum, American Helicopter Society, 1965, pp. 92-98.

12. Rainey, A.G.: Preliminary Study of Some Factors Which Affect the Stall-Flutter Characteristics of Thin Wings. NACA TN 3622, 1956.

13. Ham, N.D.: An Experimental Investigation of Stall Flutter. J. Am. Helicopter Soc., vol. 7, no. 1, Jan. 1962, pp. 3-16.

14. Carta, F.O.: Coupled Blade-Disk-Shroud Flutter Instabilities in Turbojet Engine Rotors, J. Eng. Power, vol. 89, no. 3, July 1967, pp. 419-426.

15. Mehta, U.B.: Dynamic Stall of an Oscillating Airfoil. Unsteady Aerodynamics, AGARD CP-277, AGARD, France, 1977, pp. 23-1 to 23-32.

16. Shamroth, S.J.: Calculation of Steady and Unsteady Airfoil Flow Fields via the Navier-Stokes Equations. NASA CR-3899, 1985.

17. Sankar, N.L.; and Tang, W.: Numerical Solution of Unsteady Viscous Flow Past Rotor Sections, AIAA Paper 85-0129, Jan. 1985.

18. Ham, N.D.; and Garelick, M.S.: Dynamic Stall Considerations in Helicopter Rotors. J. Am. Helicopter Soc., vol. 13, no. 2, Apr. 1968, pp. 49-55.

19. Baudu, N.; Sanger, M.; and Souquet, J.: Modelization Du Rechrochage Dynamique d'un Profile Oscillant. Paper Presented at the AAAF 10th Colloque d'Aeronautique Applique, Lille, France, Association Aeronautique et Astronautique de France, 1973.

20. Vezza, M.; and Galbraith, R.A.M.: Modeling of Unsteady, Incompressible Separation on an Aerofoil Using an Inviscid Flow Algorithm. GU-AERO-8412, Glasgow University, Scotland, 1984.

21. Spalart, P.R.; Leonard, A.; and Baganoff, D.: Numerical Simulation of Separated Flows. NASA TM-84328, 1983.

22. Lewis, R.I.; and Porthouse, D.T.C.: Recent Advances in the Theoretical Simulation of Real Fluid Flows. North East Coast Inst. Eng. Shipbuild. Trans., vol. 99, 1983, pp. 88-104.

23. Ono, K.; Kuwahara, K.; and Oshima, K.: Numerical Analysis of Dynamic Stall Phenomena of an Oscillating Aerofoil by the Discrete Vortex Approximation. 7th International Conference on Numerical Methods in Fluid Dynamics, (Lecture Notes in Physics, vol. 141) W.C. Reynold's and R.W. MacCormack, eds., Springer Verlag, 1981, pp. 310-315.

24. Katz, J.: A Discrete Vortex Method for the Nonsteady Separated Flow Over an Airfoil. J. Fluid Mech., vol. 102, Jan. 1981, pp. 315-328.

25. Rao, B.M.; Maskew, B.; and Dvorak, F.A.: Theoretical Prediction of Dynamic Stall on Oscillating Airfoils. American Helicopter Society 34th Annual National Forum, American Helicopter Society, 1978.

26. Scruggs, R.M.; Nash, J.F.; and Singleton, R.E.: Analysis of Flow Reversal Delay for a Pitching Airfoil. AIAA Paper 74-183, Jan. 1974.

27. Crimi, P; and Reeves, B.L.: A Method for Analyzing Dynamic Stall. AIAA Paper 72-37, Jan. 1972.

28. Wu, J.C.; and Wang, C.M.: Dynamic Stall of Oscillating Airfoils. American Helicopter Society 42nd Annual National Forum, American Helicopter Society, 1986.

29. Tokel, H.; and Sisto, F.: Dynamic Stall of an Airfoil with Leading Edge Bubble Separation Involving Time Dependent Reattachment. ASME Paper 78-GT-194, Aug. 1978.

30. Perumal, P.V.K.; and Sisto, F.: Lift and Moment Prediction for an Oscillating Airfoil with a Moving Separation Point. J. Eng. Power, vol. 96, no. 4, Oct. 1974, pp. 372-378.

31. Yashima, S.; and Tanaka, H.: Torsional Flutter in Stalled Cascade. J. Eng. Power, vol. 100, no. 2, Apr. 1977, pp. 317-325.

32. Chi, R.M.: Separated Flow Unsteady Aerodynamic Theory, J.Aircr., vol. 22, no. 11, Nov. 1985, pp. 956-964.

33. Carta, F.O., et al.: Analytical Study of Helicopter Rotor Stall Flutter. American Helicopter Society 26th Annual National Forum, American Helicopter Society, 1970.

34. Gross, D.W.; and Harris, F.D.: Prediction of Inflight Stalled Airloads from Oscillating Airfoil Data. American Helicopter Society 25th Annual National Forum, American Helicopter Society, 1969.

35. Gormont, R.E.: A Mathematical Model of Unsteady Aerodynamics and Radial Flow for Application to Helicopter Rotors. USAAMRDL-TR-72-67, May 1973.

36. Johnson, W.; and Ham, N.D.: On the Mechanism of Dynamic Stall. J. Am. Helicopter Soc., vol. 17, no. 4, Oct. 1972, pp. 36-45.

37. Bielawa, R.L.: Synthesized Unsteady Airfoil Data with Applications to Stall Flutter Calculations. American Helicopter Society 31st Annual National Forum, American Helicopter Society, 1975.

38. Gangwani, S.T.: Synthesized Airfoil Data Method for Prediction of Dynamic Stall and Unsteady Airloads. NASA CR-3672, 1983. (Also, Gangwani, S.T.: Prediction of Dynamic Stall and Unsteady Airloads for Rotor Blades. J. Am. Helicopter Soc., vol. 27, no. 4, Oct. 1982, pp. 57-64.)

39. Tran, C.T.; and Petot, D.: Semi-Empirical Model for the Dynamic Stall of Airfoils in View of the Application to the Calculation of Responses of a Helicopter Blade in Forward Flight. Vertica, vol. 5, no. 1, 1981, pp. 35-53.

40. Beddoes, T.S.: A Synthesis of Unsteady Aerodynamic Effects Including Stall Hysteresis. Vertica, vol. 1, no. 2, 1976, pp. 113-123.

41. Ericson, L.E.;and Reding, J.P.: Dynamic Stall of Helicopter Blades, J. Am. Helicopter Soc., vol. 17, no. 1, Jan. 1972, pp. 11-19.

42. Philippe, J.J.: Dynamic Stall: An Example of Strong Interaction Between Viscous and Inviscid Flows. NASA TM-75447, 1978.

43. Beddoes, T.S.: Prediction Methods for Unsteady Separated Flows. Special Course in Unsteady Aerodynamics. AGARD-R-679, AGARD, France, 1980, pp. 15-1 to 15-11.

44. Johnson, W.: Helicopter Theory, Chapter 16, Priceton University Press, 1980.

45. McCroskey, W.J.: The Phenomenon of Dynamic Stall. NASA TM-81264, 1981.

46. Carr, L.W.: Dynamic Stall Progress in Analysis and Prediction. AIAA Paper 85-1769, Aug. 1985.

47. Galbraith, R.A.M.; and Vezza, M.: Methods of Predicting Dynamic Stall. Paper Presented at the British Wind Energy Conf., Cambridge, U.K., Apr. 1986.

48. Young, W.H. Jr.: Fluid Mechanics Mechanism in the Stall Process for Helicopters. NASA TM-81956, 1981.

49. Carta, F.O.: A Comparison of the Pitching and Plunging Response of an Oscillating Airfoil. NASA CR-3172, 1979.

50. Fukushima, T.; and Dadone, L.U.: Comparison of Dynamic Stall Phenomena for Pitching and Vertical Translation Motions. NASA CR-2693, 1977.

51. Ericson, L.E.; and Reding. J.P.: The Difference Between the Effects of Pitch and Plunge on Dynamic Airfoil Stall. Ninth European Rotorcraft Forum, Sept. 13-15, Stresa, Italy, 1983, pp. 8-1 to 8-8.

52. Bisplinghoff, R.L.; Ashley, H.; and Halfman, R.L.: Aeroelasticity, Addison-Wesley, 1955, p. 272.

53. Rogers, J.P.: Applications of an Analytic Stall Model to Time-History and Eigenvalue Analysis of Rotor Blades. J. Am. Helicopter Soc., vol. 29, no. 1, Jan. 1984, pp. 25-33.

54. Peters, D.A.: Toward a Unified Lift Model for use in Rotor Blade Stability Analyses, J. Am. Helicopter Soc., vol. 30, no. 3, July 1985, pp. 32-42.

55. Dowell, E.H.: Non-Linear Oscillator Models in Bluff Body Aeroelasticity. J. Sound Vib., vol. 75, no. 2, Mar. 22, 1981, pp. 251-264.

56. Liiva, J.; and Davenport, F.J.: Dynamic Stall of Airfoil Sections for High Speed Rotors. J. Amer. Helicopter Soc., vol. 12, no. 2, Apr. 1969, pp. 26-33.

57. Bielawa, R.L.. et al.: Aeroelastic Analysis for Propellers, NASA CR-3729, 1983.

58. Petot, D.: Dynamic Stall Modeling of the NACA 0012 Profile. La Rech. Aerospatiale (Engl. Transl.), no. 6, 1984, pp. 55-58.

59. Bathe, K.J.; and Wilson, E.L.: Numerical Methods in Finite Element Analysis, Prentice Hall, 1976.

60. Fanti, R.; Carta, F.O.; and Pitt, W.R.: Stall-Flutter Characteristics of Several 16-Series Cantilevered Airfoil Models. United Aircraft Corporation, Hartford, CT, R-23624-2, May 1954.

TABLE I. - DYNAMIC STALL PREDICTION METHODS

Method for predictions	Reference	Predictive capability																									
		To stall onset					Stall onset				Post stall						Motion				Other factors						
		Unsteady pressure distribution	Unsteady boundary layer	Laminar-turbulence transition	Flow reversal	Compressibility	Leading edge criterion	Trailing edge separation	Shock-wave interaction	Acoustic waves	Vorticity buildup/ shedding	Vorticity transport	Wake modeling	Induced effects of wake	Subsequent vortex shedding	Reattachment	Sinusoidal	Ramp	Plunge	Other	Sweep/3-dimensional	Reynold's number	Blade vortex interaction	Roughness, etc.	Free stream turbulence	Noise
Navier-Stokes	15	a	a	b	a	b	a	a	b	b	a	a	a	a	a	a	a	b	b	b	b	c	b	b	b	b
	16	a	a	a	a	a	a	a	b	b	a	a	a	a	a	a	b	a	b	b	b	b	b	b	b	b
	17	a	a	b	a	a	a	a	c	b	a	a	a	a	a	a	a	a	a	b	c	d	a	b	b	b
Discrete vortex	18	c	b	b	b	b	e	b	b	b	a	a	a	a	b	c	a	b	b	a	b	b	b	b	b	b
	19	a	b	b	b	b	c	b	b	b	a	a	a	a	a	b	a	b	b	b	b	b	b	b	b	b
	20	a	b	b	b	b	b	e	b	b	a	a	a	a	a	e	a	a	f	a	b	b	b	b	b	b
	21	a	f	c	f	b	c	c	b	b	a	a	a	a	a	c	a	b	b	b	b	b	b	b	b	b
	22	a	b	b	b	b	c	c	b	b	a	a	a	a	a	b	f	b	b	e	b	e	b	b	b	b
	23	a	b	b	b	b	e	e	b	b	c	a	a	a	c	c	a	b	a	b	b	b	b	b	b	b
	24	e	b	b	b	b	e	e	b	b	a	a	a	a	a	b	b	b	b	c	b	b	b	b	b	b
Zonal	25	e	e	a	b	b	b	a	b	b	b	b	e	e	b	c	a	b	b	b	b	b	b	b	b	b
	26	a	a	b	a	b	b	a	b	b	b	b	b	e	b	b	b	a	b	b	b	b	e	b	b	b
	27	c	e	a	b	b	a	a	b	b	b	b	e	e	b	a	a	a	a	a	b	b	e	b	b	b
Predominantly empirical	40	c	b	b	b	a	a	a	a	b	a	a	b	b	b	a	a	a	b	b	b	b	b	b	b	b
	38	b	b	b	b	a	a	b	b	b	a	a	b	b	b	a	a	b	a	a	a	e	b	b	b	b
	39	b	b	b	b	a	e	e	b	b	e	e	b	b	b	a	a	b	c	b	a	b	b	b	b	b
	41	b	b	b	b	e	e	e	b	b	b	b	b	b	b	c	a	a	a	b	b	b	b	b	b	b
	35	b	b	b	b	a	e	b	b	b	b	e	b	b	b	c	a	b	b	b	b	b	b	b	b	b
	36	b	b	b	b	b	e	b	b	b	b	a	b	b	b	e	b	a	b	b	b	b	b	b	b	b

[a]Good level of modeling.
[b]Not modeled.
[c]Approximate level of modeling.
[d]Unknown level of modeling.
[e]Very approximate level of modeling.
[f]Being developed.

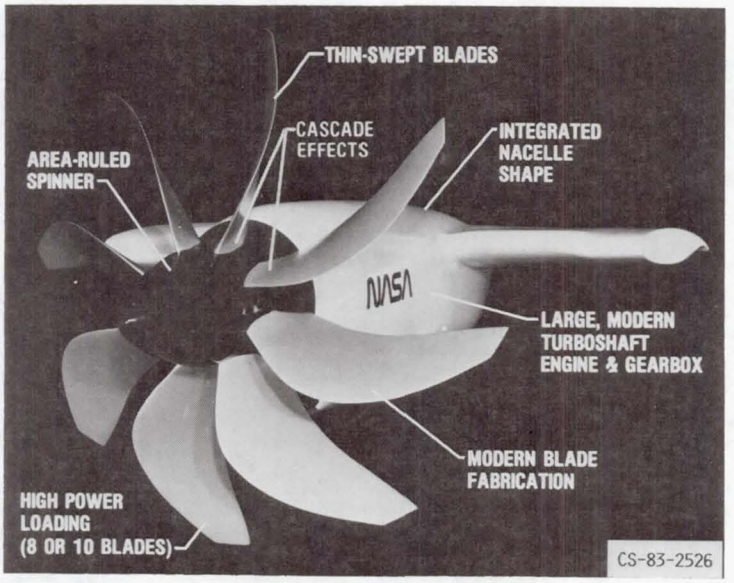

FIGURE 1. - WIND TUNNEL MODEL OF AN ADVANCED TURBOPROP.

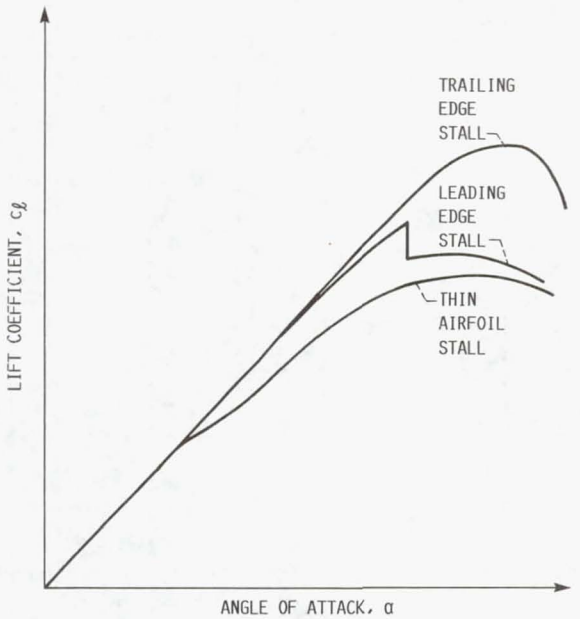

FIGURE 2. - THREE TYPES OF STALL.

CD-86-23720

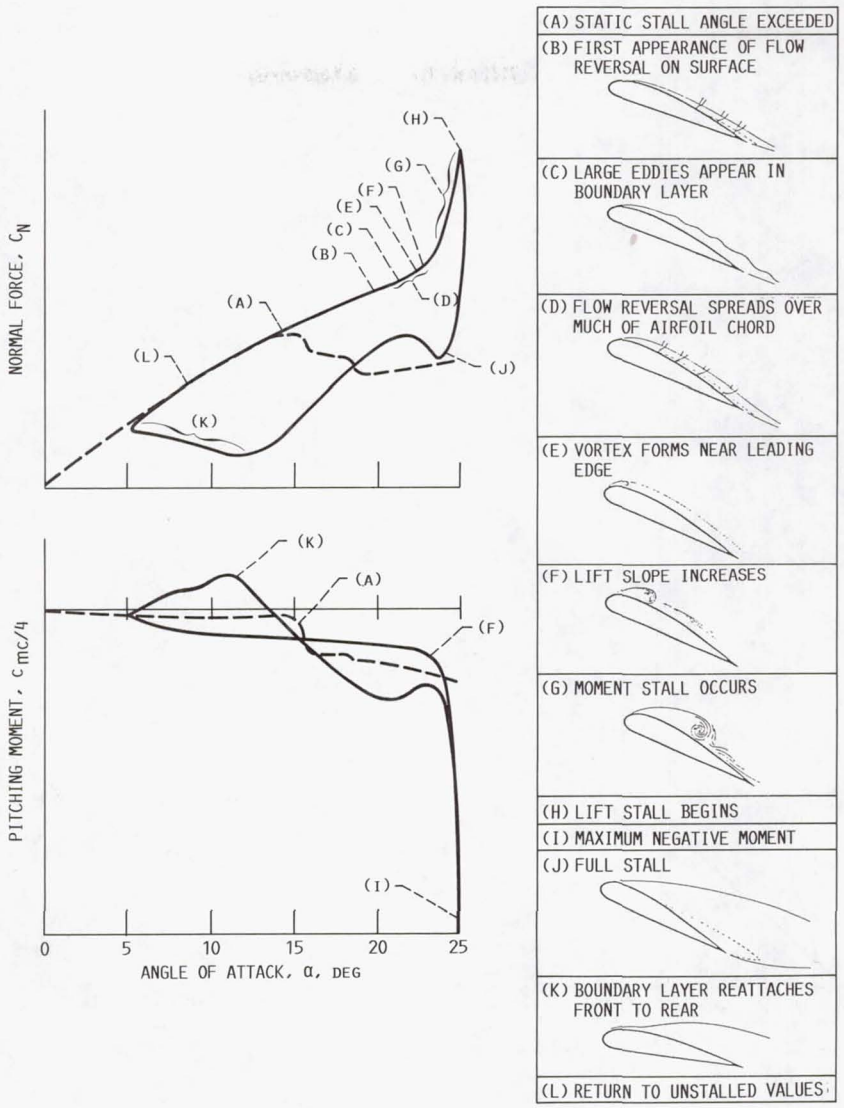

FIGURE 3. - DYNAMIC STALL EVENTS ON NACA 0012 AIRFOIL.

CD-86-23696

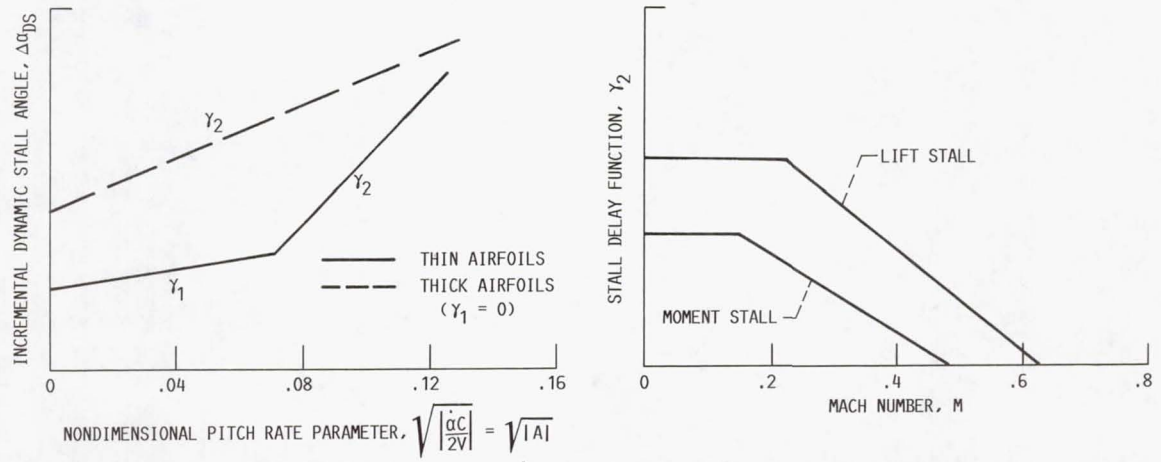

FIGURE 4. - THE VARIATION OF $\Delta\alpha_{DS}$ WITH $\dot{\alpha}$, AND THE VARIATION OF Y_2 WITH MACH NUMBER (SCHEMATIC).

CD-86-23697

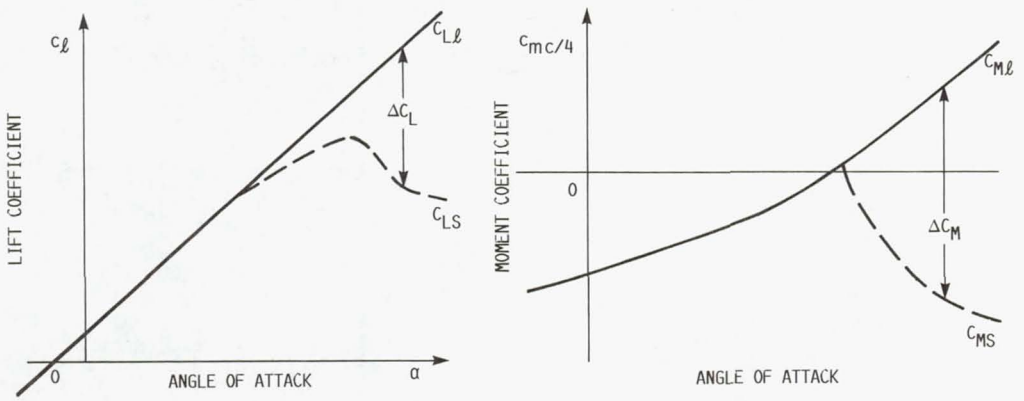

FIGURE 5. - REPRESENTATION OF $C_{L\ell}$, C_{LS}, ΔC_L, $C_{M\ell}$, C_{MS}, AND ΔC_M.

CD-86-23698

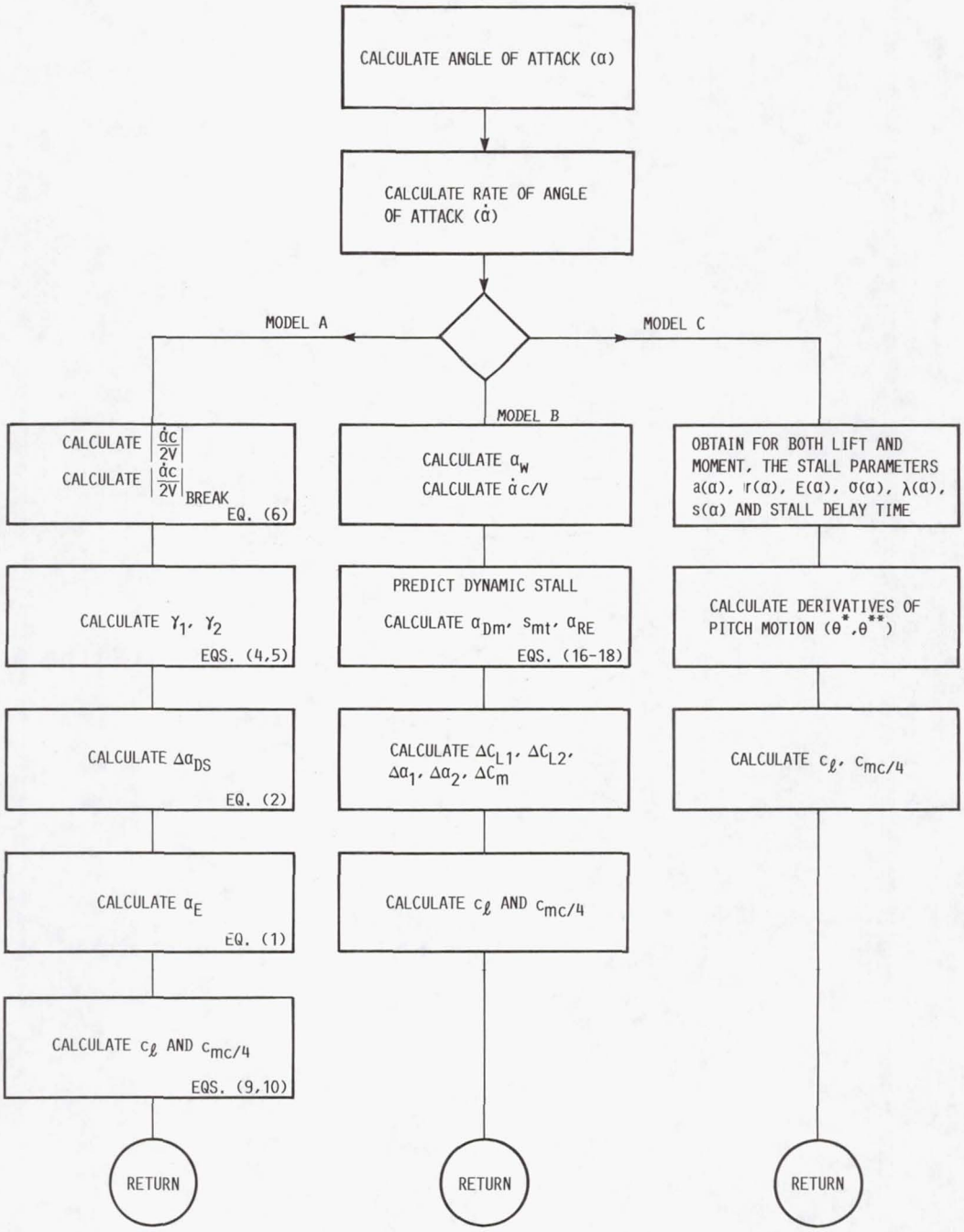

FIGURE 6. - FLOW CHART OF THE THREE DYNAMIC STALL MODELS.

CD-86-23699

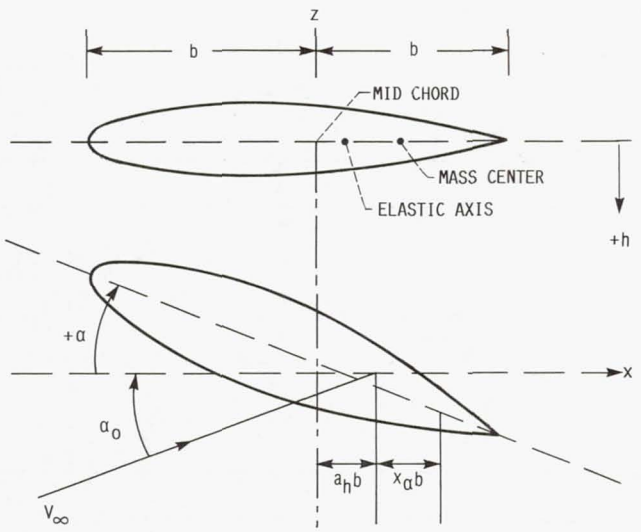

FIGURE 7. - TYPICAL SECTION MODEL.

CD-86-23723

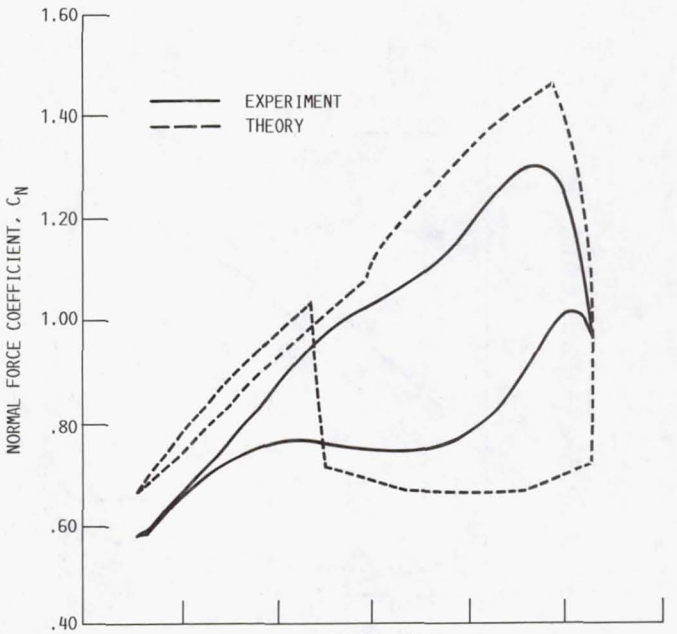

(A) NORMAL FORCE.

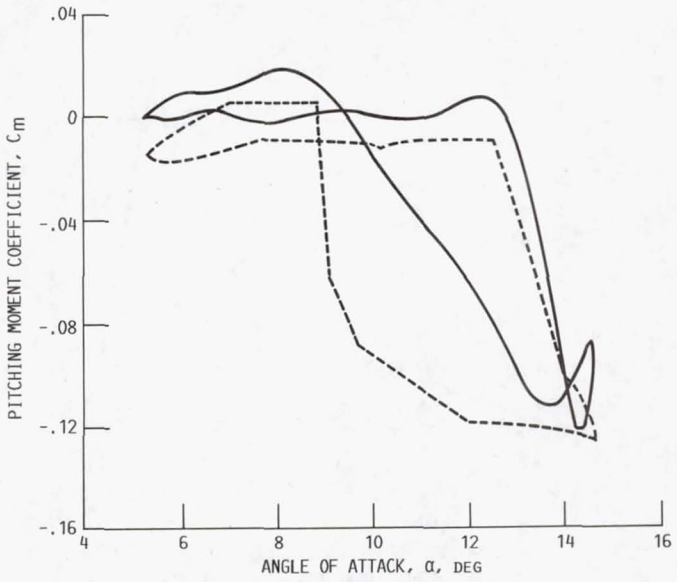

(B) PITCHING MOMENT.

FIGURE 8. - DYNAMIC COEFFICIENT LOOPS FROM MODEL A FOR NACA 0012 (MOD), $\alpha_0 = 9.93^0$, $\alpha = 4.68^0$, K = 0.064, M = 0.4.

CD-86-23725

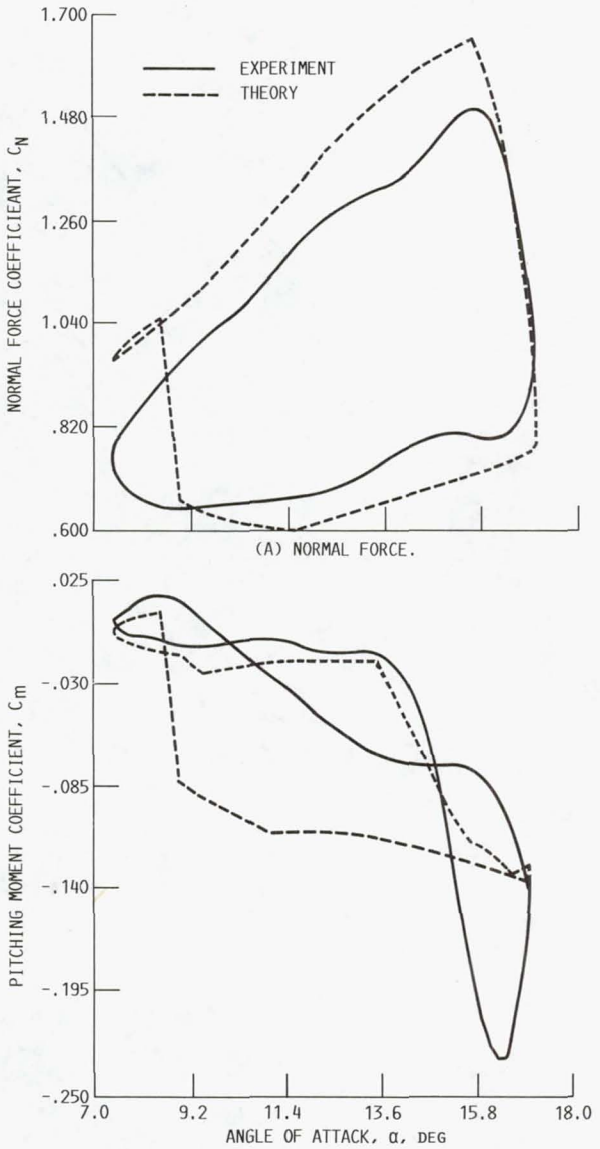

FIGURE 9. - DYNAMIC COEFFICIENT LOOPS FROM MODEL A FOR NACA 0012 (MOD), $\alpha_0 = 12.25^0$, $\bar{\alpha} = 4.8^0$, K = 0.126, M = 0.4.

CD-86-23700

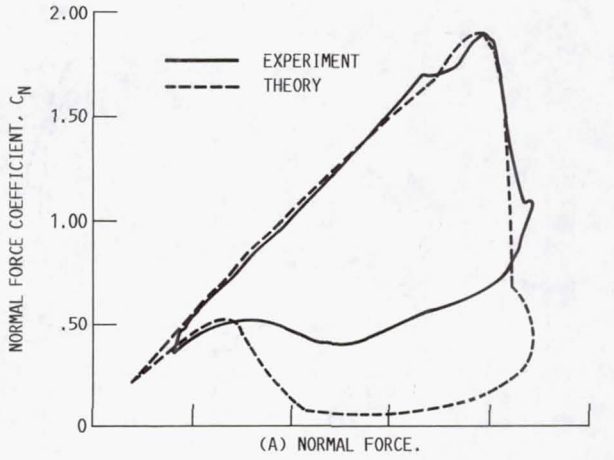

(A) NORMAL FORCE.

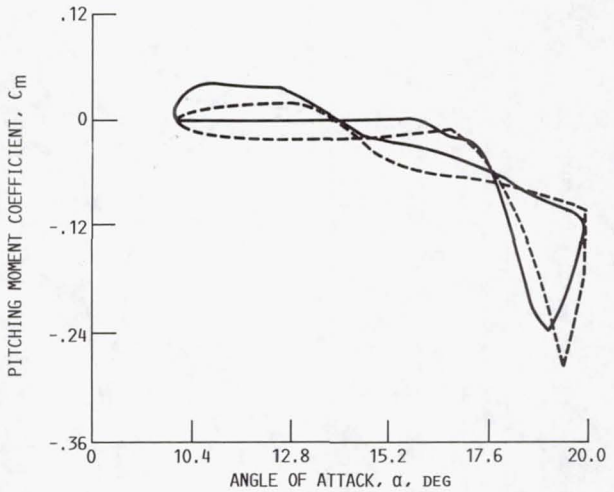

(B) PITCHING MOMENT.

FIGURE 10. - DYNAMIC COEFFICIENT LOOPS FROM MODEL B FOR NACA 0012, $\alpha_0 = 12^0$, $\bar{\alpha} = 10^0$, K = 09756, M = 0.3.

CD-86-23701

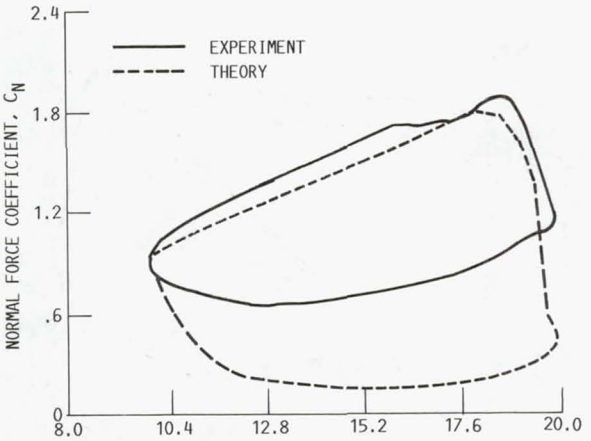

(A) NORMAL FORCE.

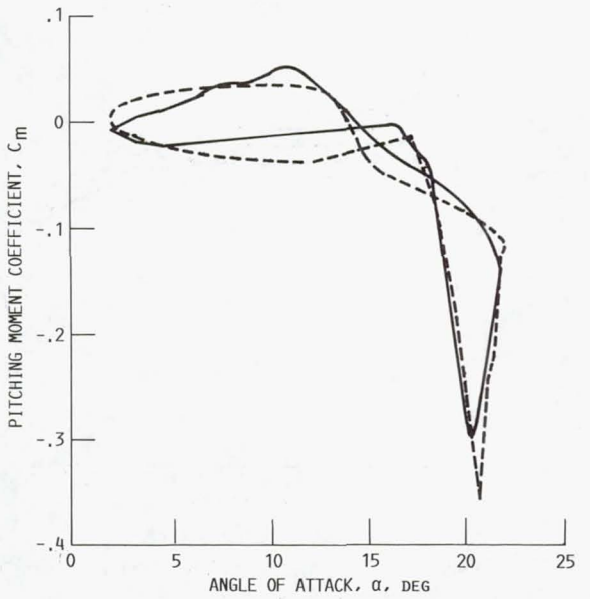

(B) PITCHING MOMENT.

FIGURE 11. - DYNAMIC COEFFICIENT LOOPS FROM MODEL B FOR NACA 0012, $\alpha_0 = 15^0$, $\bar{\alpha} = 5^0$, K = 0.151, M = 0.3.

CD-86-23716

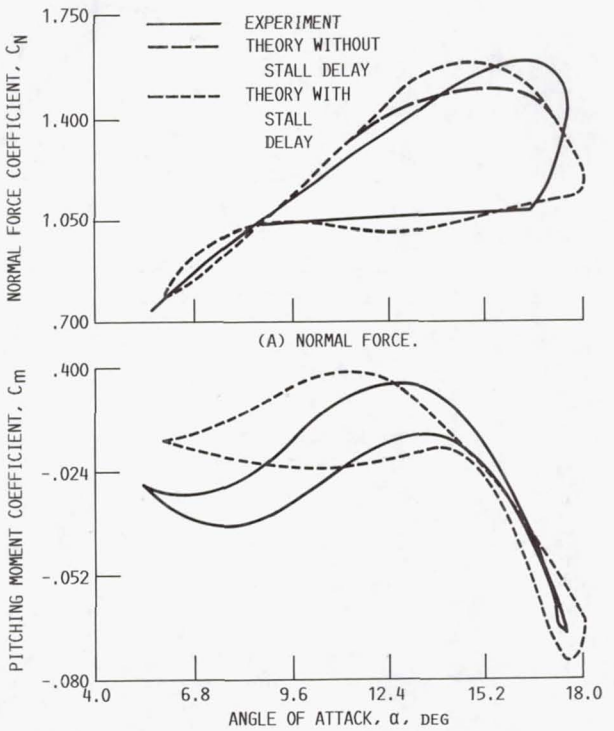

FIGURE 12. - DYNAMIC COEFFICIENT LOOPS FROM MODEL C FOR 0A212, $\alpha_o = 12^o$, $\bar{\alpha} = 6^o$, K = 0.05, M = 0.3.

CD-86-23726

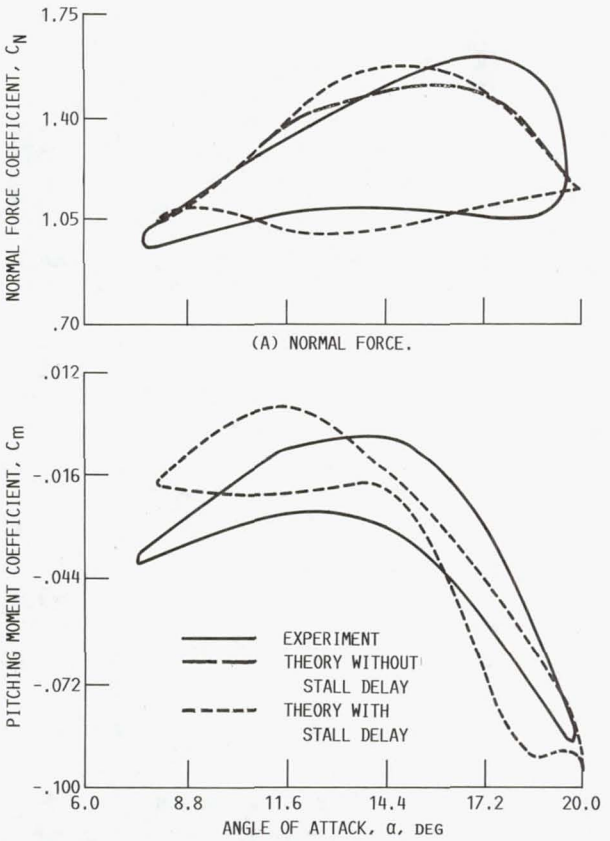

FIGURE 13. - DYNAMIC COEFFICIENT LOOPS FROM MODEL C FOR 0A212, $\alpha_0 = 14^0$, $\bar{\alpha} = 6^0$, K = 0.05, M = 0.3.

CD-86-23719

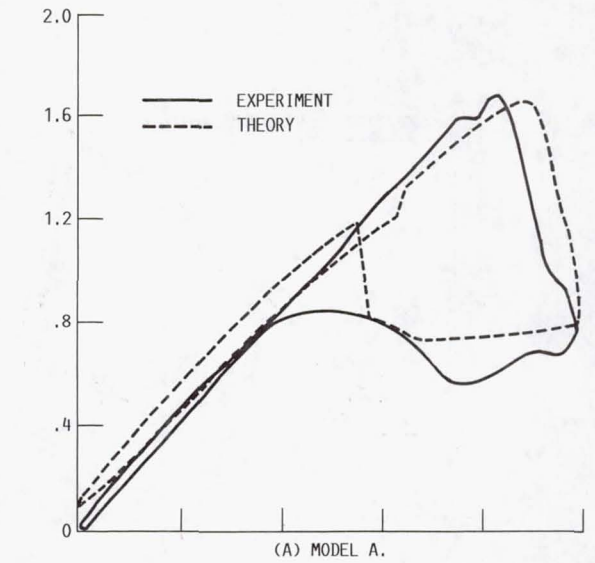

(A) MODEL A.

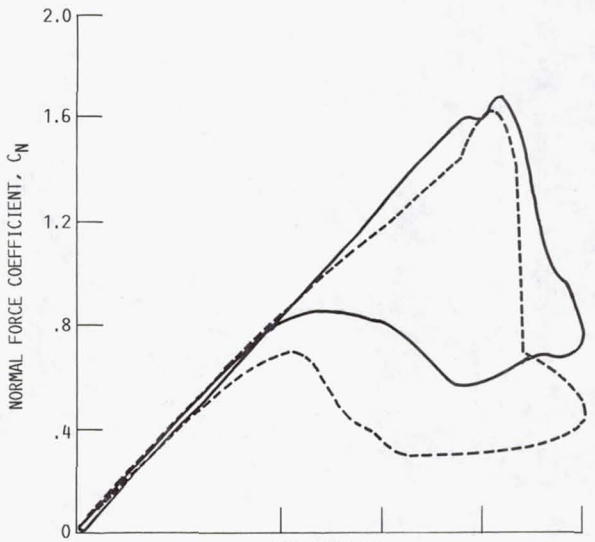

(B) MODEL B.

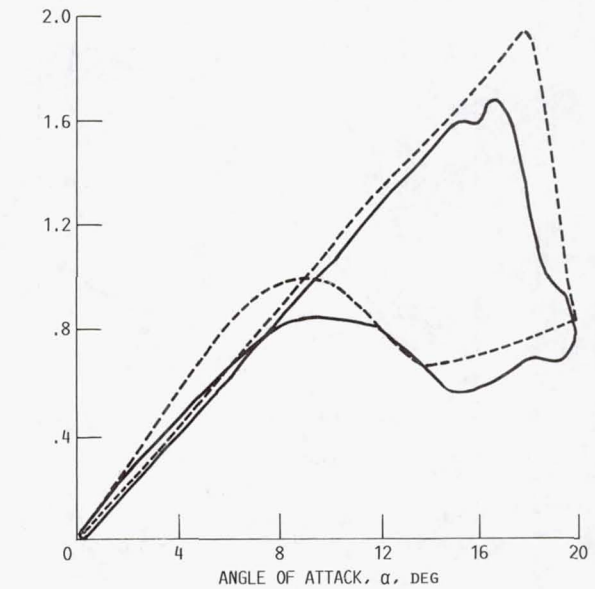

(C) MODEL C.

FIGURE 14. - DYNAMIC NORMAL FORCE COEFFICIENT LOOPS FOR NACA 0012, $\alpha_0 = 10^0$, $\bar{\alpha} = 10^0$, K = 0.04813, M = 0.3.

CD-86-23718

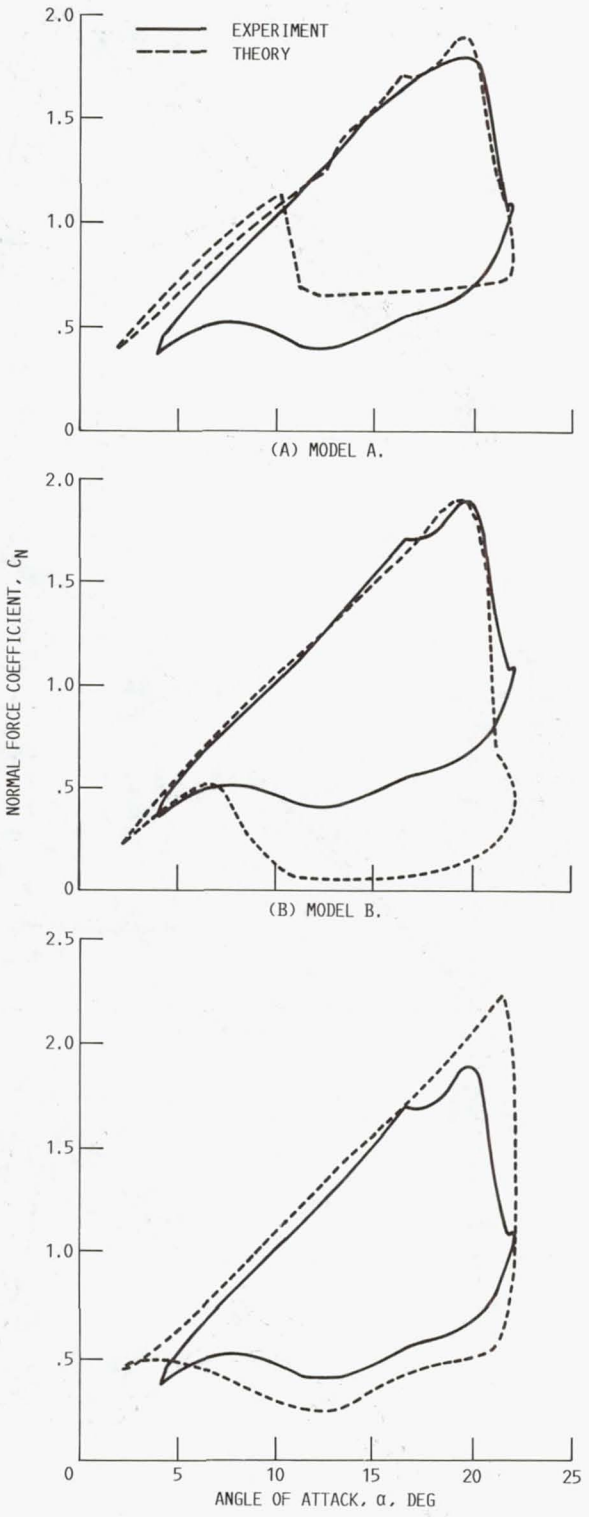

FIGURE 15. - DYNAMIC NORMAL FORCE COEFFICIENT LOOPS FOR NACA 0012, $\alpha_0 = 12^0$, $\bar{\alpha} = 10^0$, K = 0.09756, M = 0.3.

CD-86-23715

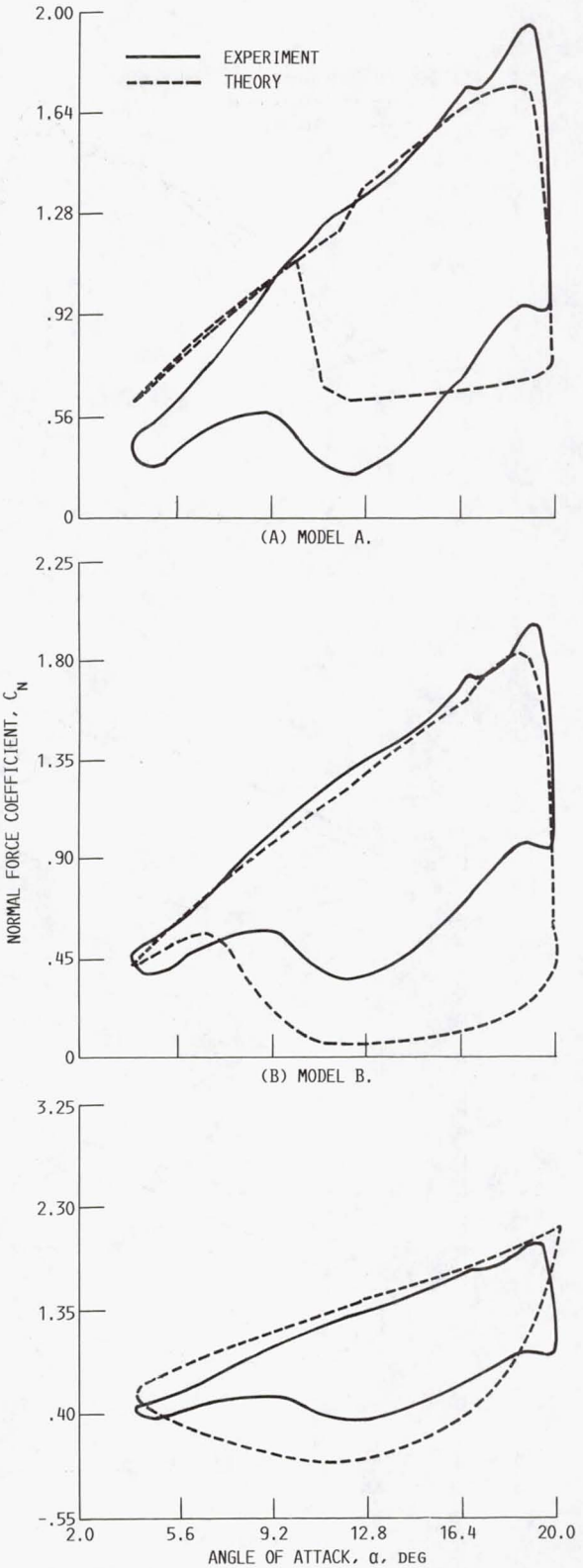

FIGURE 16. - DYNAMIC NORMAL FORCE COEFFICIENT LOOPS FOR NACA 0012, $\alpha_0 = 12^0$, $\bar{\alpha} = 8^0$, K = 0.12528, M = 0.3.

CD-86-23717

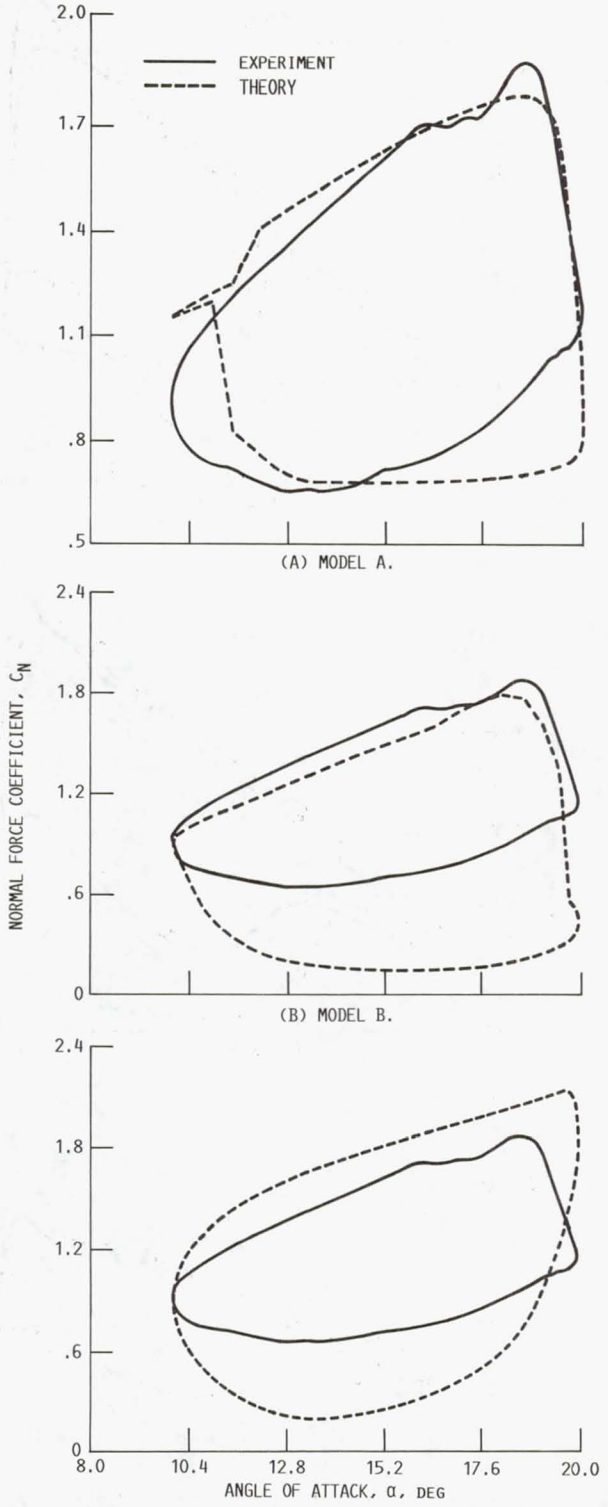

FIGURE 17. - DYNAMIC NORMAL FORCE COEFFICIENT LOOPS FOR NACA 0012, $\alpha_0 = 15^0$, $\bar{\alpha} = 5^0$, K = 0.15106, M = 0.3.

CD-86-23722

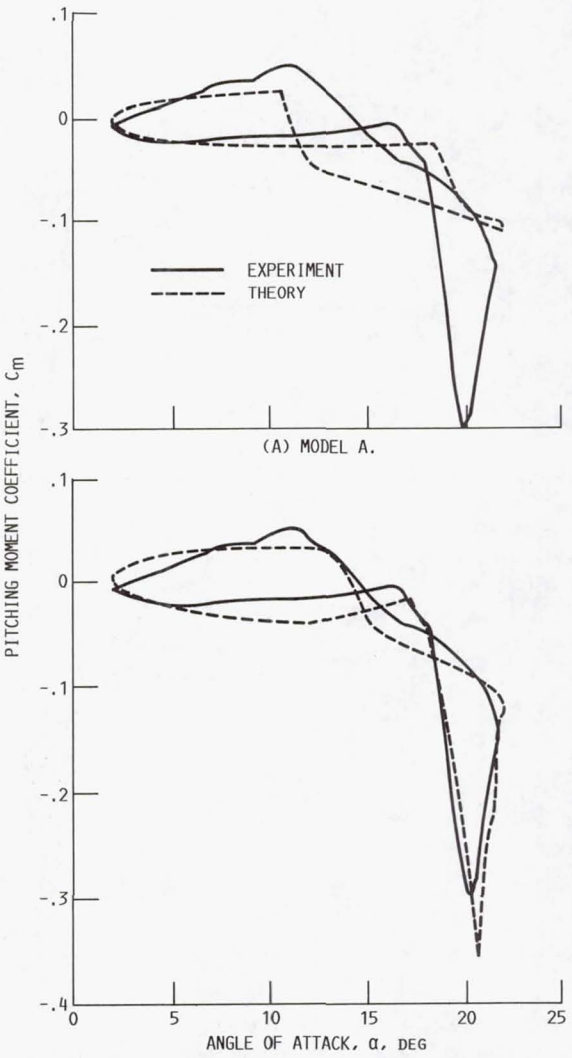

FIGURE 18. - DYNAMIC PITCHING MOMENT COEFFICIENT LOOPS FOR NACA 0012, $\alpha_o = 12^o$, $\bar{\alpha} = 10^o$, K = 0.9756.

CD-86-23702

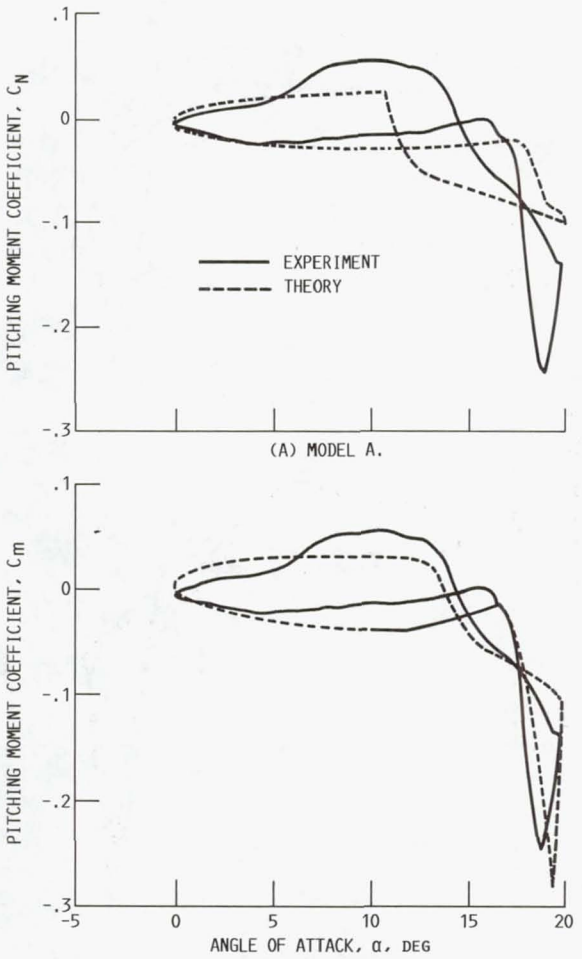

FIGURE 19. - DYNAMIC PITCHING MOMENT COEFFICIENT LOOPS FOR NACA 0012, $\alpha_0 = 10^0$, $\bar{\alpha} = 10^0$, K = 0.09633.

CD-86-23703

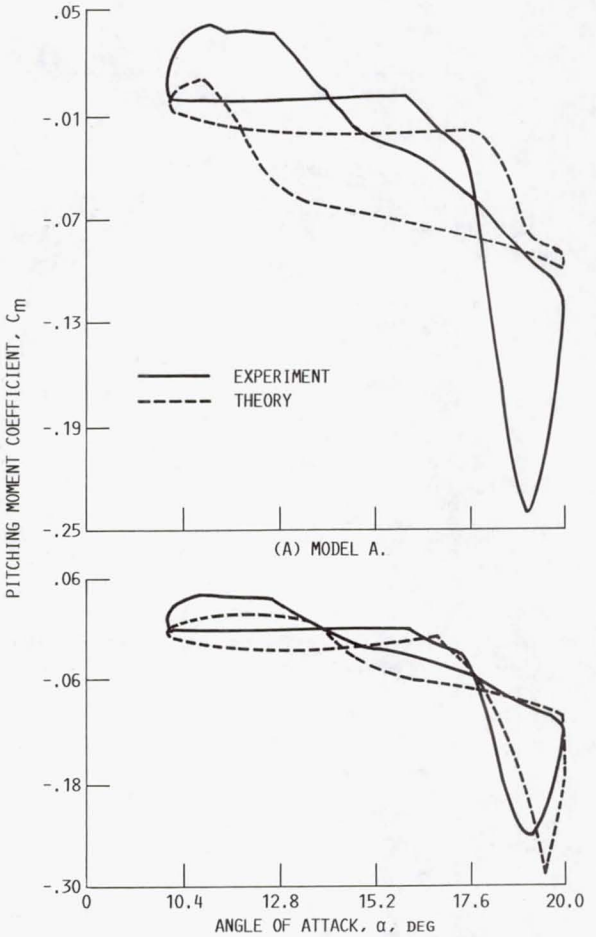

FIGURE 20. - DYNAMIC PITCHING MOMENT COEFFICIENT LOOPS FOR NACA 0012, $\bar{\alpha}_o = 15^o$, $\alpha = 5^o$, K = 0.151.

CD-86-23704

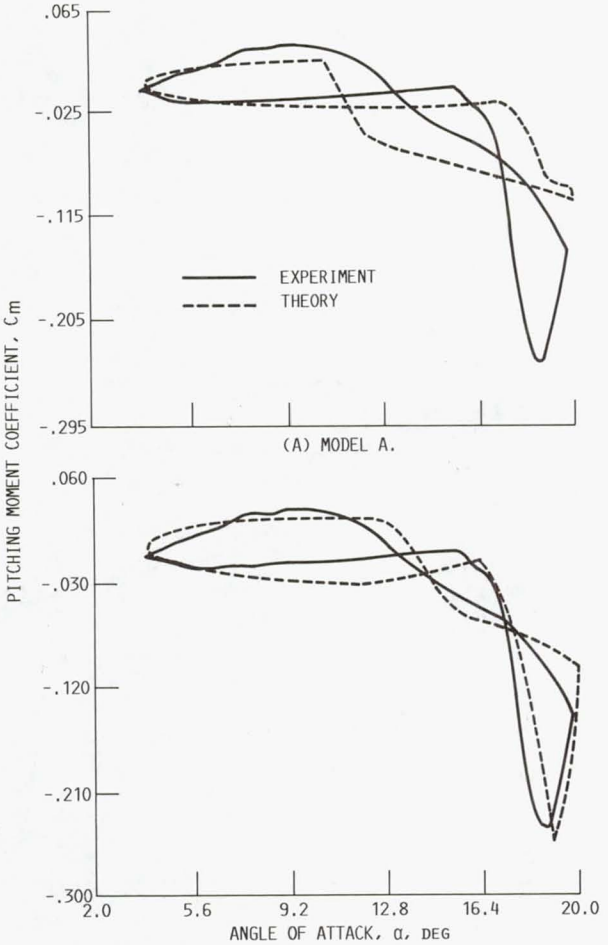

FIGURE 21. - DYNAMIC PITCHING MOMENT COEFFICIENT LOOPS FOR NACA 0012, $\alpha_0 = 12^0$, $\bar{\alpha} = 8^0$, K = 0.09675.

CD-86-23705

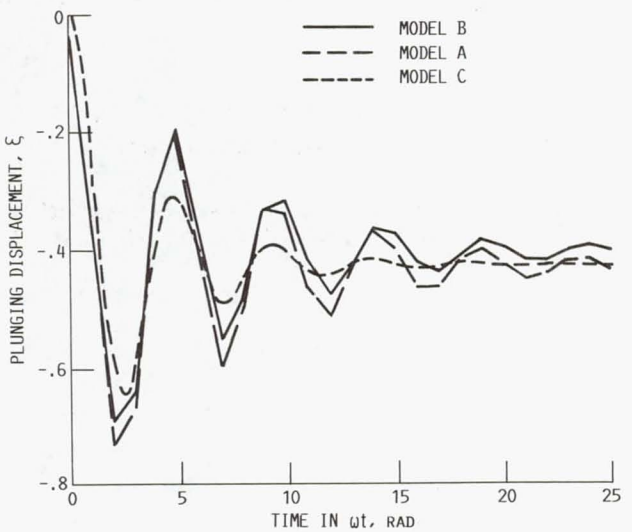

FIGURE 22. - COMPARISON OF PLUNGING DISPLACEMENT FROM THE THREE DYNAMIC STALL MODELS, NACA 0012 AIRFOIL, TYPICAL SECTION MODEL, $\alpha_0 = 4.5^0$, M = 0.3.

CD-86-23706

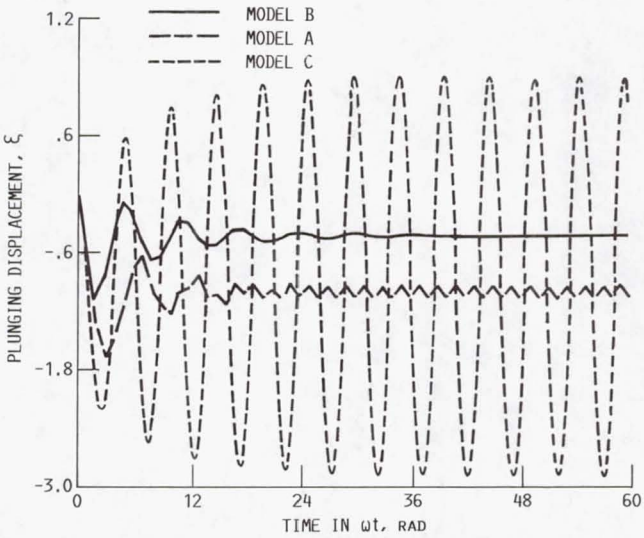

FIGURE 23. - COMPARISON OF PLUNGING DISPLACEMENT FROM THE THREE DYNAMIC STALL MODELS, NACA 0012 AIRFOIL, TYPICAL SECTION MODEL, $\alpha_0 = 15^0$, M = 0.3, $\mu = 76$.

CD-86-23724

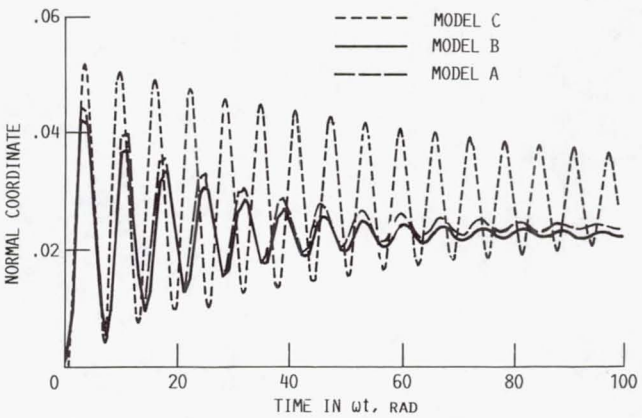

FIGURE 24. - COMPARISON OF PLUNGING DISPLACEMENT FROM THE THREE DYNAMIC STALL MODELS, NACA 0012 AIRFOIL, PLATE MODEL, $\alpha_0 = 4.5^0$, M = 0.3.

CD-86-23707

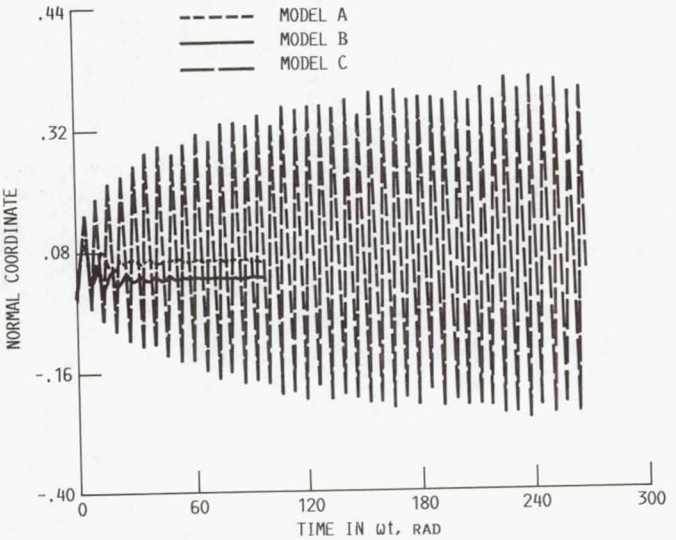

FIGURE 25. - COMPARISON OF PLUNGING RESPONSE FROM THE THREE DYNAMIC STALL MODELS, NACA 0012 AIRFOIL, PLATE MODEL, $\alpha_o = 15^o$, M = 0.3.

CD-86-23708

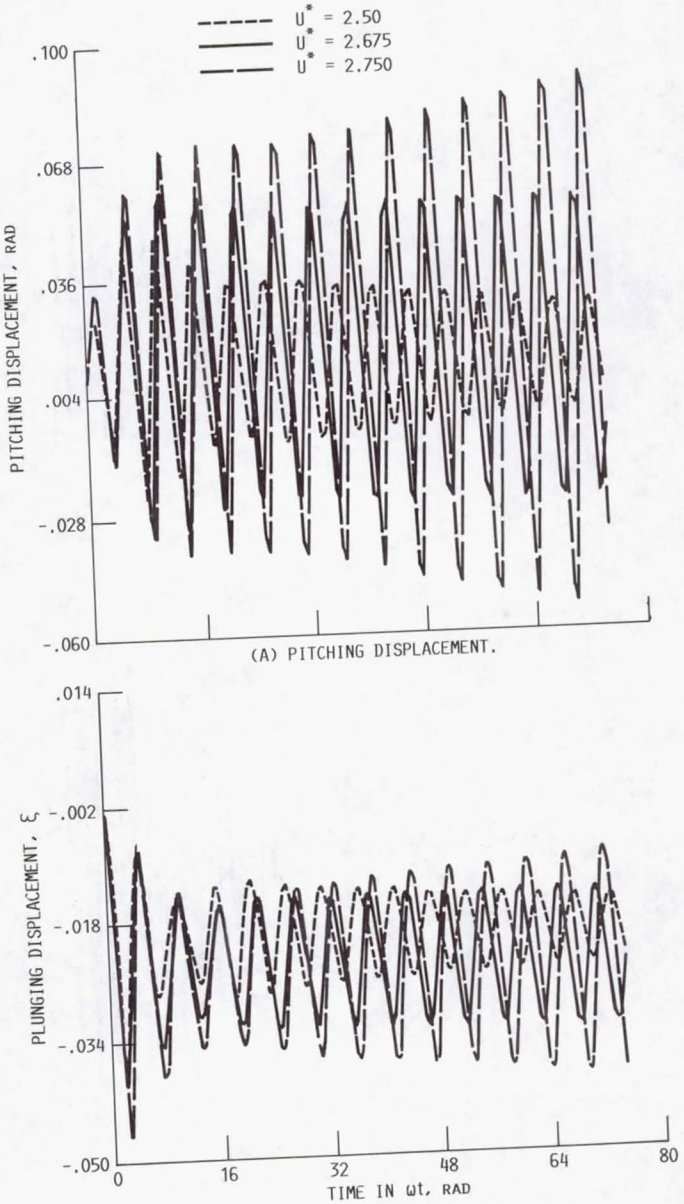

FIGURE 26. - RESPONSE OBTAINED FROM MODEL A (TYPICAL SECTION) $\alpha_0 = 4.5^0$.

CD-86-23709

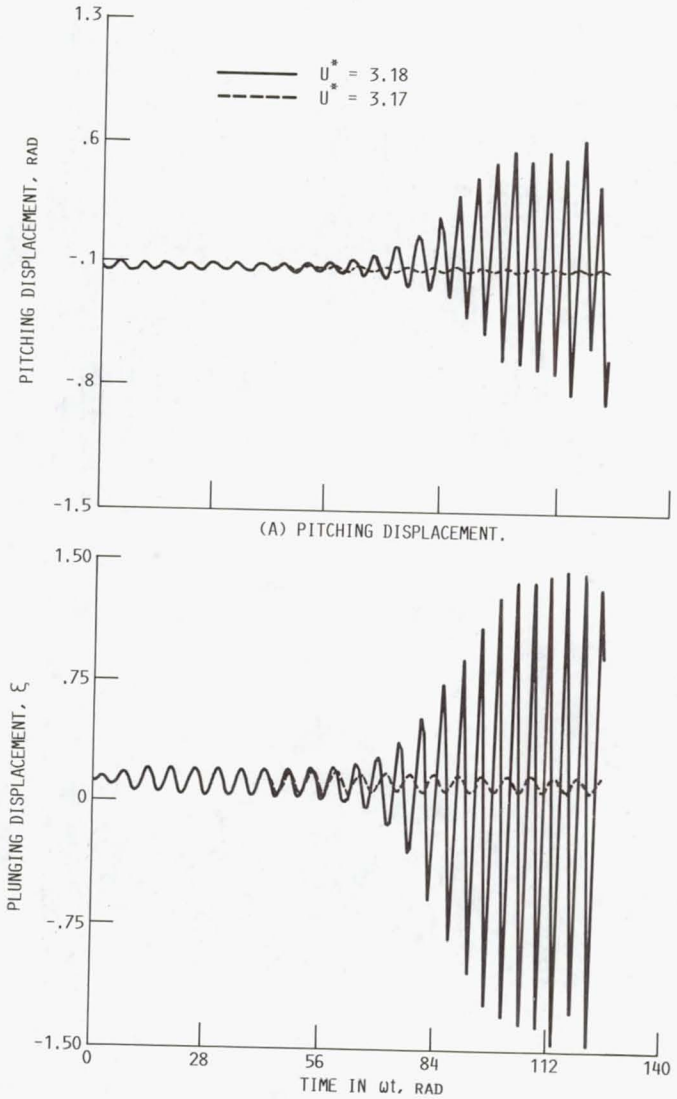

FIGURE 27. - RESPONSE OBTAINED FROM MODEL B (TYPICAL SECTION) $\alpha_o = 4.5^o$.

CD-86-23721

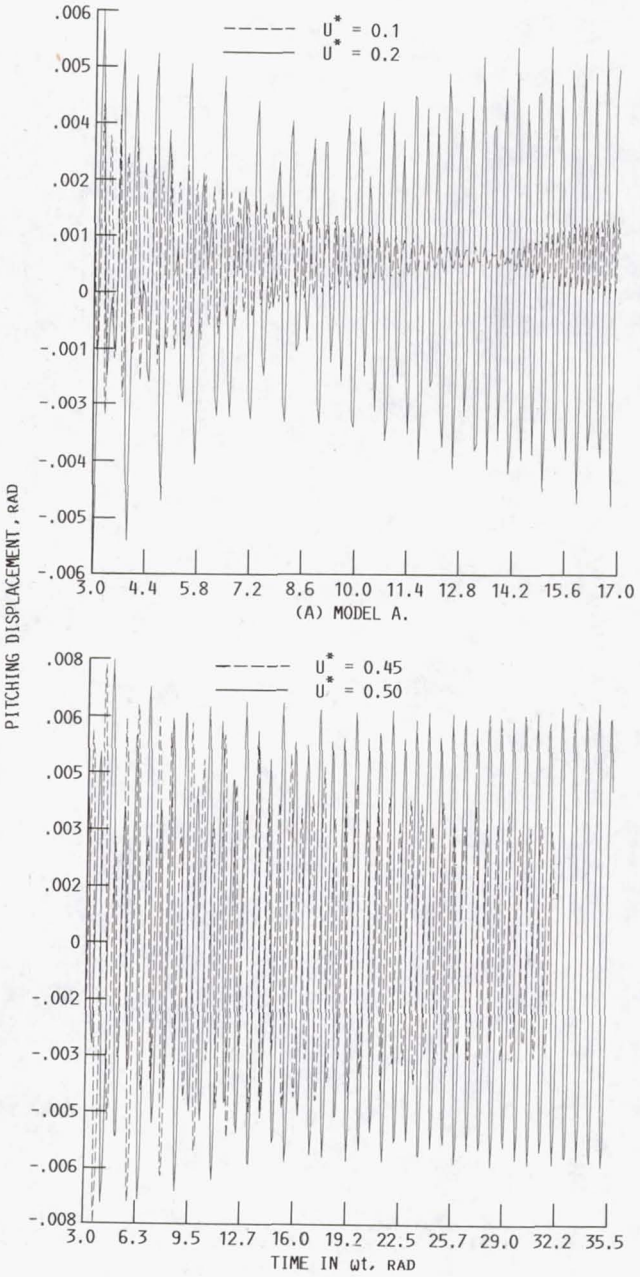

FIGURE 28. - PITCHING DISPLACEMENT RESPONSE (TYPICAL SECTION) $\alpha_0 = 15^0$.

CD-86-23693

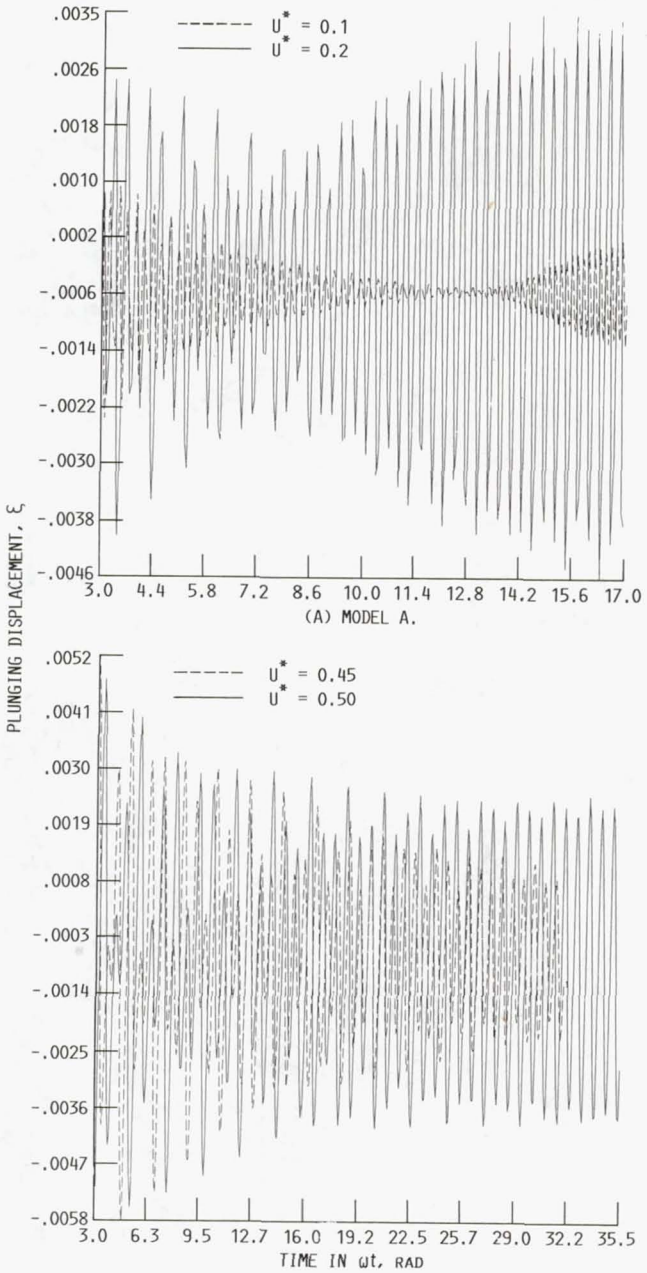

FIGURE 29. - PLUNGING DISPLACEMENT RESPONSE (TYPICAL SECTION) $\alpha_0 = 15^0$.

CD-86-23695

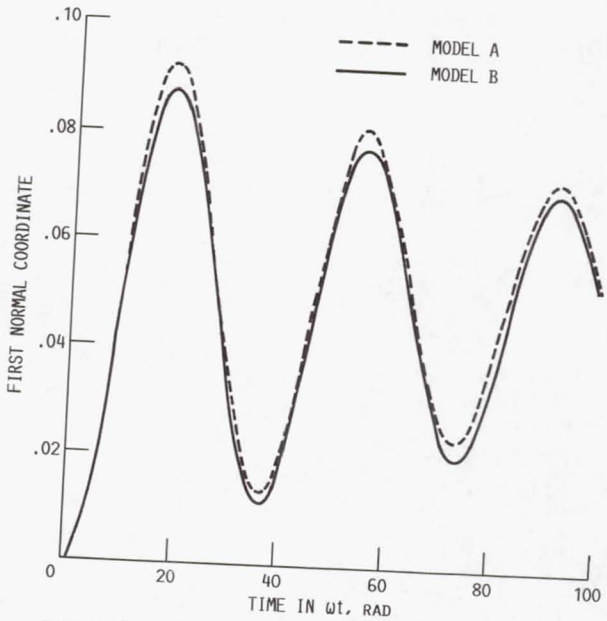

FIGURE 30. - FIRST NORMAL COORDINATE RESPONSE, PLATE MODEL, $\alpha_o = 4.5^o$, M = 0.3.

CD-86-23710

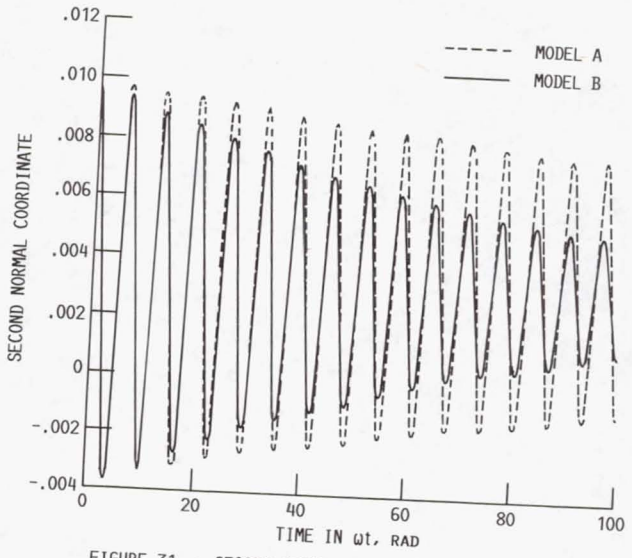

FIGURE 31. - SECOND NORMAL COORDINATE RESPONSE, PLATE MODEL, $\alpha_o = 4.5^o$, M = 0.3.

CD-86-23711

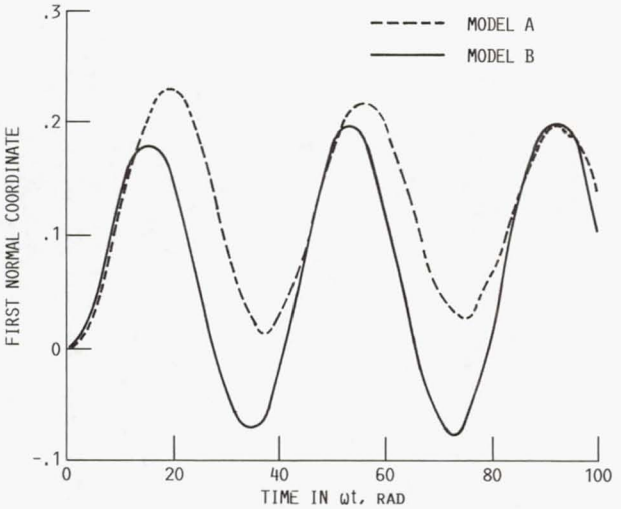

FIGURE 32. - FIRST NORMAL COORDINATE RESPONSE, PLATE MODEL, $\alpha_o = 15^o$, M = 0.3.

CD-86-23712

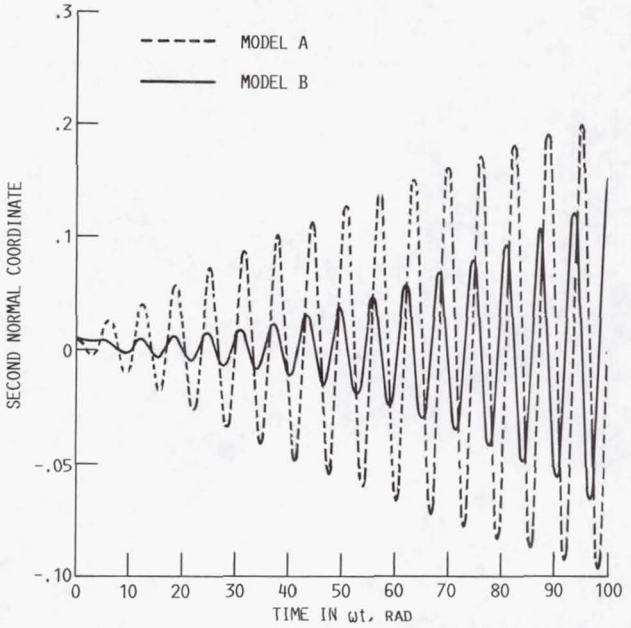

FIGURE 33. - SECOND NORMAL COORDINATE RESPONSE, PLATE MODEL, $\alpha_0 = 15^0$, M = 0.3.

CD-86-23713

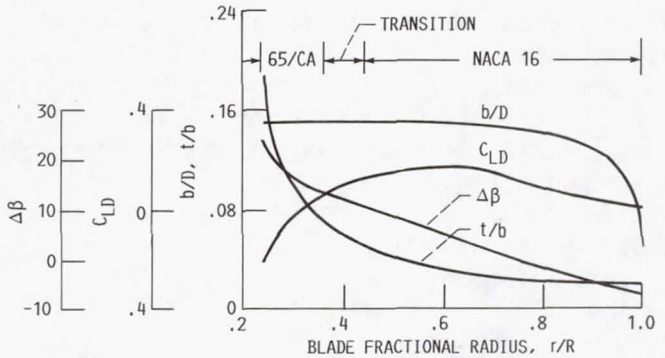

FIGURE 34. - VARIATION OF PROPELLER DESIGN PARAMETERS WITH BLADE RADIUS FOR THE UNSWEPT SR-2 PROPELLER.

CD-86-23714

1. Report No.	2. Government Accession No.	3. Recipient's Catalog No.
NASA TM-88917		

4. Title and Subtitle	5. Report Date
A Comparative Study of Some Dynamic Stall Models	March 1987
	6. Performing Organization Code: 535-03-01

7. Author(s)	8. Performing Organization Report No.
T.S.R. Reddy and K.R.V. Kaza	E-3342
	10. Work Unit No.

9. Performing Organization Name and Address	11. Contract or Grant No.
National Aeronautics and Space Administration Lewis Research Center Cleveland, Ohio 44135	
	13. Type of Report and Period Covered: Technical Memorandum

12. Sponsoring Agency Name and Address	14. Sponsoring Agency Code
National Aeronautics and Space Administration Washington, D.C. 20546	

15. Supplementary Notes

T.S.R. Reddy, The University of Toledo, Toledo, Ohio 43606 and NASA Resident Research Associate; K.R.V. Kaza, NASA Lewis Research Center.

16. Abstract

Three semi-empirical aerodynamic stall models are compared with respect to their lift and moment hysteresis loop predication, limit cycle behavior prediction, easy implementation, and feasibility in developing the parameters required for stall flutter prediction of advanced turboprops. For the comparison of aeroelastic response prediction including stall, a typical section model and a plate structural model are considered. The response analysis includes both plunging and pitching motions of the blades. In model A, a correction to the angle of attack is applied when the angle of attack exceeds the static stall angle. In model B, a synthesis procedure is used for angles of attack above static stall angles and the time history effects are accounted through the Wagner function. In both models the lift and moment coefficients for angles of attack below stall are obtained from tabular data for a given Mach number and angle of attack. In model C, referred to as the ONERA model, the lift and moment coefficients are given in the form of two differential equations, one for angles below stall and the other for angles above stall. The parameters of these equations are nonlinear functions of the angle of attack. The effects of vortex-shedding, an important feature of dynamic stall, are not considered in model A, accurately considered in model B, and approximately considered in model C. However, it is observed that the high frequency, low amplitude oscillations, sweep, and high subsonic Mach number operating environment of advanced turboprops favor light stall conditions where the effect of vortex-shedding is less severe. This permits the use of simple models like models A and C in the stall flutter analysis of advanced turboprops.

17. Key Words (Suggested by Author(s))	18. Distribution Statement
Separated flow; Dynamic stall; Stall flutter; Response	Unclassified - unlimited STAR Category 39

19. Security Classif. (of this report)	20. Security Classif. (of this page)	21. No. of pages	22. Price*
Unclassified	Unclassified	78	A05

*For sale by the National Technical Information Service, Springfield, Virginia 22161